CHEMISTRY & SUSTAINABILITY

CHEMSUSCHEM

ENERGY & MATERIALS

Reprint

© Wiley-VCH Verlag GmbH & Co. KGaA, Weinheim

A Journal of ChemPubSoc Europe

WILEY-VCH

www.chemsuschem.org

ChemPubSoc Europe
DOI: 10.1002/cssc.201802873
CHEMSUSCHEM Minireviews

Iridium-Based Catalysts for Solid Polymer Electrolyte Electrocatalytic Water Splitting

Chao Wang[+],*[a] Feifei Lan[+],[a] Zhenfeng He,[b] Xiaofeng Xie,[c] Yuhong Zhao,[a] Hua Hou,[a] Li Guo,[a] Vignesh Murugadoss,[d] Hu Liu,[d, e] Qian Shao,[f] Qiang Gao,*[g] Tao Ding,*[h] Renbo Wei,*[i] and Zhanhu Guo*[d]

Chemical energy conversion/storage through water splitting for hydrogen production has been recognized as the ideal solution to the transient nature of renewable energy sources. Solid polymer electrolyte (SPE) water electrolysis is one of the most practical ways to produce pure H_2. Electrocatalysts are key materials in the SPE water electrolysis. At the anode side, electrode materials catalyzing the oxygen evolution reaction (OER) require specific properties. Among the reported materials, only iridium presents high activity and is more stable. In this Minireview, an application overview of single iridium metal and its oxide catalysts—binary, ternary, and multicomponent catalysts of iridium oxides and supported composite catalysts—for the OER in SPE water electrolysis is presented. Two main strategies to improve the activity of an electrocatalyst system, namely, increasing the number of active sites and the intrinsic activity of each active site, are reviewed with detailed examples. The challenges and perspectives in this field are also discussed.

1. Introduction

Climate change, pollution, and the scarcity of fossil fuels require our society to pursue clean and renewable energy sources. Hydrogen is considered to be the most abundant and promising energy carrier because of its high efficiency, lack of environmental pollution, and so forth. Nowadays, water electrolysis is the most attractive renewable resource for hydrogen production. Electricity can be derived from solar energy, wind energy, water conservancy, tidal energy, geothermal energy, and so forth.[1–5]

Regarding water electrolysis, solid polymer electrolyte (SPE) water electrolysis has been extensively investigated.[5–8] The main advantages of SPE water electrolysis are fast kinetics of the cathodic hydrogen evolution reaction (HER) and high voltage efficiencies at high current densities. The main challenge arising from high energy consumption limits its large-scale industrial applications, mainly owing to the higher overpotential of the sluggish oxygen evolution reaction (OER). Moreover, the lack of stable electrocatalysts remains challenging. Under operation conditions, few electrocatalysts can present adequate stability. Noble IrO_2 has excellent corrosion resistance and high catalytic activity for OER,[8] whereas the high price of IrO_2 has limited its applications. In the appropriate synthetic protocol, selecting the right material to dope or support the catalyst can

[a] Prof. C. Wang,[+] F. Lan,[+] Prof. Y. Zhao, Prof. H. Hou, Prof. L. Guo
Advanced Energy Materials and Systems Institute
College of Materials Science and Engineering
North University of China, Taiyuan, 030051 (PR China)
E-mail: wangchao_nuc@126.com

[b] Prof. Z. He
National Demonstration Center for Experimental Chemical Engineering
Comprehensive Education, School of Chemical Engineering and Technology
North University of China, Taiyuan 030051 (PR China)

[c] Prof. X. Xie
INET, Tsinghua University
Beijing, 100084 (PR China)

[d] V. Murugadoss, Dr. H. Liu, Prof. Dr. Z. Guo
Integrated Composites Laboratory (ICL)
Department of Chemical & Biomolecular Engineering
University of Tennessee, Knoxville, TN 37996 (USA)
E-mail: zguo10@utk.edu

[e] Dr. H. Liu
Key Laboratory of Materials Processing and Mold (Zhengzhou University)
Ministry of Education, National Engineering Research Center
for Advanced Polymer Processing Technology
Zhengzhou University, Zhengzhou, 450002 (PR China)

[f] Prof. Q. Shao
College of Chemical and Environmental Engineering
Shandong University of Science and Technology
Qingdao, Shandong, 266590 (PR China)

[g] Dr. Q. Gao
Center for Nanophase Materials Sciences, Oak Ridge National Laboratory
P.O. Box 2008, Oak Ridge, TN 37831 (USA)
E-mail: gaoq@ornl.gov

[h] Prof. T. Ding
College of Chemistry and Chemical Engineering
Henan University, Kaifeng 475004 (PR China)
E-mail: dingtao@henu.edu.cn

[i] Prof. R. Wei
Research Branch of Advanced Functional Materials, School of Materials and Energy, University of Electronic Science and Technology of China
Chengdu, 611731 (PR China)
E-mail: weirb10@uestc.edu.cn

[+] These authors contributed equally to this work.

The ORCID identification number(s) for the author(s) of this article can be found under:
https://doi.org/10.1002/cssc.201802873.

© 2019 Wiley-VCH Verlag GmbH & Co. KGaA, Weinheim

effectively reduce the amount of anode metals and, meanwhile, improve the corrosion resistance of the electrode.

The main feature of SPE water electrolysis technology lies in replacing traditional caustic solution electrolytes with SPE. The solid polymer is a perfluorosulfonic acid proton exchange membrane (PEM; commonly Nafion). Sulfonic acid groups can deliver hydronium ions and become a good conductor after flooding, and hydrogen ions have a good conduction. A PEM satisfies numerous physical criteria, including 1) good ionic conductivity and thermal conductivity, 2) poor electronic conductivity, 3) good chemical and mechanical stability, 4) good thermal stability, 5) ease of manufacture and production in the form of large-surface membranes of homogeneous thickness, and 6) low gas solubility.[9] A PEM serves as both electrolyte and separator. The SPE water electrolysis principle is illustrated in Figure 1. The cathode and anode reactions occurring at the

Chao Wang, born in 1987 in Beijing, engages mainly in research into polymer flame-retardant materials, fuel cells, and ion-exchange membranes. He has hosted one National Science Foundation for Young Scientists of China and participated in the Key International S&T Cooperation Projects of the Ministry of Science and Technology.

Qiang Gao works in the scanning probe microscopy (SPM) group at Oak Ridge National Laboratory. His projects involve the development of in situ SPM in liquid for energy technologies. He obtained his Ph.D. at CNRS, France under the supervision of Prof. Dr. François Béguin. Then, he worked on in situ and ex situ spectroscopy techniques development for water splitting electrocatalysts at the Max Planck Institute for Chemical Energy Conversion, Germany under the supervision of Prof. Dr. Robert Schlögl. His research interests include materials and electrolytes for advanced energy storage and conversion, and in operando spectroscopy and microscopy in quantifying interfacial and pore scale fluid-solid interactions.

Tao Ding received his B.S. degree in 1995 and his M.S. in 2002 from Henan University, and his Ph.D. in 2006 from Beijing University of Chemical Technology. He then began his academic career at the School of Chemistry and Chemical Engineering of Henan University. Since 2011, he has been a Professor at Henan University. His main research activities focus on the preparation and applications of functional nanocomposites and flame-retardant materials centered around polyformaldehyde and polypropylene.

Renbo Wei is an Associate Professor at the School of Materials and Energy, University of Electronic Science and Technology of China, Chengdu, China. After receiving his B.S. from Jilin University in 2010, he completed his Ph.D. at Tsinghua University under the supervision of Prof. Xiaogong Wang for work on the design, synthesis, and properties of polymers. During his postdoctoral work, he extended the application of the synthesized polymers for electronic applications and detection of gases. His current research interests are related to the synthesis, electrical properties, and applications of functional materials and their composites.

Zhanhu Guo is an Associate Professor in the Department of Chemical and Biomolecular Engineering at the University of Tennessee, Knoxville, USA. He obtained his Ph.D. in Chemical Engineering from Louisiana State University (2005) and received three years (2005–2008) of postdoctoral training in the Mechanical and Aerospace Engineering Department at the University of California Los Angeles. Dr. Guo chaired the Composite Division of the American Institute of Chemical Engineers (2010–2011) and directs the Integrated Composites Laboratory (ICL). His current research focuses on multifunctional nanocomposites for transportation, safety, information, catalysis, energy harvesting and storage, electronic devices, and environmental remediation applications.

© 2019 Wiley-VCH Verlag GmbH & Co. KGaA, Weinheim

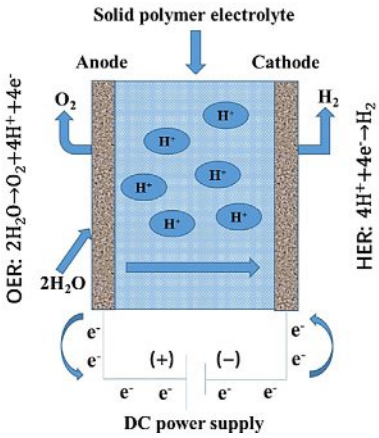

Figure 1. Cross-section illustration of a SPE water electrolysis cell. DC = direct current.

SPE water electrolysis electrodes can be described by Equations (1) and (2), respectively:

$$4\,e^- + 4\,H^+ \rightarrow 2\,H_2 \uparrow \quad (1)$$

$$2\,H_2O \rightarrow 4\,H^+ + 4\,e^- + O_2 \uparrow \quad (2)$$

Water electrolysis at the anode produces O_2 and four protons near the electrode surface for each oxygen molecule. Hydrogen ions through the PEM generate H_2 gas near the cathode. The electrocatalysts are directly attached to the membrane to form the SPE composite membrane electrode. The selective separation of the proton membrane enables an integrated structure to reduce the voltage drop of the electrolyte, and thus, has high energy efficiency and improves the current efficiency. The only liquid used in the electrolyzer is deionized water, which will reduce corrosion of the equipment and extend the service life. Nevertheless, the higher production cost limits its large-scale application.

To evaluate the performance of the catalysts, the most important parameters are their activity and stability. The key factors restricting the commercialization of H_2 production are cost and the performance of the catalysts. Thus, the research and application of catalysts are directly related to the commercial prospect of electrolyzing hydrogen from SPEs.

In the SPE water electrolysis cell, a platinum metal catalyst with acid stability and hydrogen evolution catalytic activity is the most suitable cathode for an electrocatalyst because of the strongly acidic nature (equivalent to 10% H_2SO_4) after the PEM absorbs water. The cathode for the HER in SPE water electrolysis has a low overpotential. Widely used cathodes, to date, are noble-metal platinum catalysts, including Pt/C,[10–13] Pt nanoparticles (NPs)/carbon nanofibers (CNFs),[14] Pt/graphitic nanofibers (GNF),[15] Pt–Fe, or Pt–C,[16] because Pt element has an incompletely filled d orbital, and the outermost electron structure of $5d^96s^1$ and suitable atomic radius of 177 pm favor the adsorption of H atoms and the desorption of H_2, that is, faster kinetics of electron reduction to H_2 results in a lower activation energy, and thus, lower hydrogen evolution potential. To reduce the amount of Pt and increase its electrochemical specific surface area, it has been usually prepared as Pt particles and supported on a porous carbon substrate, for example, Pt/C catalyst particles.

Herein, we summarize (in Table 1) and discuss current issues and recent developments in IrO_2-based catalysts for the OER in SPE water electrolysis to extract guidelines for developing electrocatalysts with high activity, low cost, and high stability.

2. Progress in Catalysts for the OER

2.1. OER catalysts

The overpotential of the OER is much higher than that of the HER.[17,18] Accordingly, the OER has been intensively studied to elucidate the reaction mechanism and stability issues and to reduce the overpotential of the OER electrode during water electrolysis. The standard electrode potential for the OER is 1.23 V versus a reversible hydrogen electrode (RHE), but most metal electrodes dissolve before reaching this potential; only a few metals and their oxides present adequate stability. Figure 2 shows the oxygen evolution polarization curves of different metals and their oxides in acidic solution.[19] The oxygen evolution current values of different material surfaces can differ by several orders of magnitude at a certain overpotential. Ruthenium and RuO_2 electrodes are the best electrocatalysts for oxygen generation in acidic solution. Figure 3 shows the relationship between the metal oxide overpotential and the enthalpy of oxidation of different valence oxides at a current density of 1 mA cm^{-2}.[19–21] Clearly, RuO_2 and IrO_2 are promising oxygen anode catalysts, appearing at the top of the curve. Both have the most suitable metal–oxygen bond strength and are the most conducive to the OER with the lowest overpotential.[22–25]

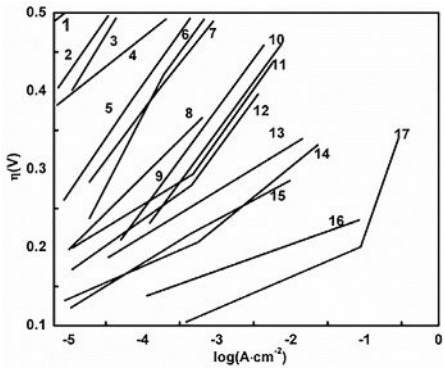

Figure 2. Schematic overpotential versus log *i* curves for oxygen evolution on various metals and oxides from acid solutions. Modified from Ref. [19]. Key: 1. Fe_3O_4; 2. Pt; 3. PbO_2; 4. $SrFeO_3$; 5. Ni; 6. β-MnO_2; 7. Pt/MnO_2; 8. (111) RuO_2; 9. β-MnO_2 + Mn_2O_3; 10. PtO_2; 11. Ir; 12. Co_3O_4; 13. IrO_2; 14. 30% RuO_2 (TiO_2); 15. RuO_2 (compact); 16. Ru; 17. RuO_2.

Pure RuO_2 catalysts as dimensionally stable anodes (DSAs) for the OER have been reported with a very short lifetime due to the easy conversion of RuO_2 into RuO_4 at high potentials. For example, Hodnik et al. used highly sensitive in situ meas-

© 2019 Wiley-VCH Verlag GmbH & Co. KGaA, Weinheim

Table 1. A summary of publications on OER activity with respect to the materials, methods, and components used in SPE water electrolysis.[a]

Catalyst anode	cathode	Loading [mg cm^{-2}] anode	cathode	Membrane	Cell area [cm^2]	P [atm]	T [°C]	E [V] at 1 A cm^{-2}	Anode catalyst preparation	Water flow rate	Ref.
IrO_2	Pt	2.5	0.4	–	7	1	90	1.7	–		[33]
IrO_2	Pt	0.5	0.25	N.115	25	1	80	1.72		200 mL h^{-1}	[35]
IrO_2	Pt/C-Baltic	2	2	Aquivion (120 μm)	6.25	3 bar	120	1.57	hydrolysis		[38]
IrO_2	10 %Pt/C_{XC72}	2	0.4	–	5		80	1.65			[40]
IrO_2	Pt/C	3	0.5	N.112	5	1	80	1.63	colloid		[42]
IrO_2	Pt/C	3	0.5	N.112	5	1	80	1.66	Adams		[42]
IrO_2	40 %Pt/C	1.5	0.5	N.212	5	1	80	1.62	Adams		[44]
IrO_2	30 %Pt/C_{XC72}	3	0.6	N.115	5	1	80	1.7	colloid		[46]
IrO_2/CP	Pt/C	0.1	0.4	N.212	4	1	90	1.6	electrodeposition		[54]
IrO_2(SBA-15)	40 %Pt/C_{JM}	1.5	1	N.115	5	1	90	1.629	hard template		[57]
Ir-ND/ATO	46Pt/C_{TKK}	total noble-metal loading: 1		N.212	5	1	80	1.67	reduction	1.5 mL min^{-1}	[59]
$Ru_{0.9}Ir_{0.1}O_2$	46.1 %Pt/C_{TKK}	2.5	0.4	N.115	25	10 bar	60	1.88	thermal decomposition		[66]
$Ru_{0.8}Ir_{0.2}O_2$	46.1 %Pt/C_{TKK}	2.5	0.4	N.115	5	1	25	1.8	thermal decomposition		[67]√
$Ir_{0.2}Ru_{0.8}O_2$	28.4 %Pt/C	total noble-metal loading: 1.7		N.1035	5	1	80	1.622	Adams		[70]
$Ir_{0.7}Ru_{0.3}O_x$	30 %Pt/C	1.5	0.5	N.115	5	1	90	1.57	Adams	4 mL min^{-1}	[72]√
$Ir_{0.7}Ru_{0.3}O_x$	30 %Pt/C_{XC72}	1.5	0.5	Aquivion (120 μm)	5	1	90	1.56	Adams	2 mL min^{-1}	[77]
$Ir_{0.5}Ru_{0.5}O_x$	–	3	–	N.115	5	1	80	–	–	40 mL min^{-1}	[78]
$Ir_{0.7}Ru_{0.3}O_x$	30 %Pt/C_{XC72}	total noble-metal loading: 1.6		Aquivion (90 μm)	5	1	80	1.58	Adams	4 mL min^{-1}	[79]
$Ru_{0.8}Ir_{0.2}O_2$	46.1 %Pt/C_{TKK}	1–1.6	0.2	N.117	25	1	80	1.739	coprecipitation	–	[83]
$Ir_{0.6}Ru_{0.4}O_2$	20 %Pt/C_{XC72}	2	0.4	N.115	5	–	80	1.567	aqueous hydrolysis	5 mL min^{-1}	[91]√
IrO_2	20 %Pt/C_{XC72}	2	0.4	N.115	5	–	90	1.61	modified polyol	–	[93]
$Ir_{0.8}Sn_{0.2}O_2$	20 %Pt/C_{XC72}	2	0.4	N.115	5	–	80	1.642	polyol	–	[93]
$Ir_{0.4}Ru_{0.6}O_2$	28.4 %Pt/C_{TKK}	1.5	0.5	N.1035	5	–	80	1.646	Adams	–	[96]
$Ir_{0.4}Ru_{0.6}Mo_xO_y$	28.4 %Pt/C_{TKK}	1.5	0.5	N.1035	5	–	80	1.606	Adams	–	[96]
$Ru_{0.3}Ir_{0.7}O_2/Pt_{0.15}$	40 %Pt/C_{JM}	1.8	0.3	N.117	20	–	60	1.76	two-step method		[100]
$Ir_{0.52}Sn_{0.48}O_2$	70 %Pt/C	1.5	0.57	N.115	5	–	80	1.631	surfactant-assisted method		[102]
IrO_2/SnO_2 (2:1)	40 %Pt/C_{JM}	1.5	0.5	N.212	1	–	80	1.64	Adams		[103]
Pt–IrO_2/SnO_2	40 %Pt/C_{JM}	1.2	0.5	N.212	1.5	1	80	1.533	chemical reduction		[114]
IrO_2: 10 wt % F	Pt $black_{SA}$	–	–	N.115	5×5	1	50	1.95	Adams		[117]
RuO_2/ATO	50 %Pt/C_{AA}	10	1	N.212	–	–	80	1.56	colloid	1–3 cm^3 mL^{-1}	[130]
90 % IrO_2/ATO	20 %Pt/C_{AA}	2	0.5	N.115	1	1	80	1.73	Adams		[133]
80 % IrO_2/ATO	20 %Pt/C_{AA}	2	0.5	N.115	1	1	80	1.74	Adams		[133]
60 % IrO_2/ATO	20 %Pt/C_{AA}	2	0.5	N.115	1	1	80	1.8	Adams		[133]
40 % IrO_2/ATO	20 %Pt/C_{AA}	2	0.5	N.115	1	1	80	1.96	Adams		[133]
60 % $IrO_2/TiO_{2.(R200M)}$	Pt	0.9	0.5	N.117	4	3 bar	120	1.67	Adams		[145]
50 % IrO_2/Ti	46 %Pt/C_{TKK}	0.2	0.25	N.115	25	1	80	1.73	–	–	[154]
Ir/Ebonex	20 %Pt/C_{XC72}	0.2	0.2	N.117	25	1	80	1.74	sol–gel	–	[160]
40I/TN-20	40 %Pt/C_{JM}	2.5	0.5	N.117	3.645	1	80	2.027	EISA	40 mL min^{-1}	[162]
40Ir/TV-20	40 %Pt/C_{JM}	2.5	0.5	N.117	3.645	1	80	2.015	EISA	40 mL min^{-1}	[165]
90 % IrO_2/ITO	20 %Pt/C_{AA}	2	0.5	N.115	1	1	80	1.74	Adams		[166]
60 % IrO_2/ITO	20 %Pt/C_{AA}	2	0.5	N.115	1	1	80	1.78	Adams		[166]
IrO_2	20 %Pt/C_{AA}	2	0.5	N.115	1	1	80	1.73	Adams		[166]
Ir/TiC (40 wt % Ir)	40 %Pt/C_{JM}	1.5	1	N.112	20	1	80	1.8		10 mL min^{-1}	[168]
20 % Ir/TiC	Pt	1.5	1	N.112	20	1	80	1.85		10 mL min^{-1}	[169]
$Ir_{0.7}Ru_{0.3}O_x$(EC)	40 % Pt/C	1	0.4	N.212	50	1	80	1.68			[178]
$Ir_{0.7}Ru_{0.3}O_x$(TT)	40 % Pt/C	1	0.4	N.212	50	1	80	1.74			[178]

[a] CP = carbon paper, ATO = antimony-doped tin oxide, ITO = indium tin oxide, EC = electrochemical leaching, TT = thermally treated, JM = Johnson Matthey; N. = Nafion; AA = Alfa Aesar; SA = Sigma–Aldrich; TKK = Tanaka; C = carbon Vulcan XC-72; √ = iR correction; EISA = evaporation-induced self-assembly. 1 atm = 101325 Pa, 1 bar = 10^5 Pa.

© 2019 Wiley-VCH Verlag GmbH & Co. KGaA, Weinheim

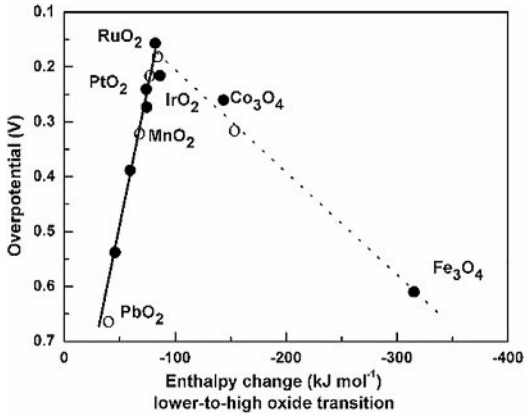

Figure 3. Relationship between metal oxide overpotential and enthalpy of conversion of different valence oxides at 1 mA cm^{-2}. Modified from Ref. [19].

urements of concentration determined by means of inductively coupled plasma (ICP) MS to study the dissolution behavior of Ru and its oxides on the nanoscale in acidic media, and revealed, for the first time, that severe dissolution took place due to the OER.[26] Moreover, OER activity displayed an inverse relationship with the measured dissolution. Cherevko et al. demonstrated an increase of dissolution in the order of $IrO_2 \leqq RuO_2$;[27] the SPE electrolytic cell anode catalyst usually contains Ir or IrO_2 as the main active component. Previous studies have shown that, under acidic conditions, the OER activity of IrO_2 is only slightly lower than that of RuO_2, whereas IrO_2 has a service life of 20 times longer than that of RuO_2.[28–30] Unfortunately, the low reserves of iridium and its high cost are major obstacles for the large-scale application of SPE water electrolysis.[31] Consequently, selecting appropriate materials to dope or load the catalyst will effectively reduce the amount of anode metals, improve the corrosion resistance of the electrode, and reduce the cost.

2.1.1. Single iridium metal and its oxide catalysts

IrO_x is the most widely used anode catalyst for the OER because of its higher stability and corrosion resistance, although its electrochemical activity is slightly lower than that of RuO_2.[32–39] Fine powders of IrO_2 can be synthesized through a variety of approaches, including the Adams fusion method,[40–45] colloid protocol,[42,46,47] sulfite complex route to films,[48] magnetron sputtering,[49–51] reduction,[52] electrode deposition, and thermal decomposition.[50,53,54] For instance, in the case of the Adams method, Wang et al. investigated the effect of precursor calcination temperature on the catalytic activity of the catalysts.[44] The calcination temperature affected the catalytically active area and electrocatalytic activity by affecting the size of the catalyst and the valence of iridium. With increasing temperature, the crystallite size and crystallinity increased, and the crystal-specific surface area and electrocatalytic activity decreased. The conductivity increased as the temperature increased. An increase in both crystallinity and particle size was observed with increasing treatment time, which was known to contribute to a decrease in active surface area of the electrocatalysts. For example, Song et al. compared the Adams and colloid synthetic methods to obtain IrO_2.[42] Consequently, the colloid method performs better than the Adams method. This result may be due to a better dispersion of electrocatalyst in the polymer electrolyte and higher crystallinity with higher conductivity of electrocatalysts. The more clearly discernible diffraction peaks for IrO_2 (colloid) samples than those for IrO_2 (Adams) indicated that the former possessed a slightly higher crystallinity. The average size of individual crystallites obtained through both methods, IrO_2 (Adams) and IrO_2 (colloid), was about 5.5 nm, as calculated from the Scherrer equation. IrO_2 (colloid) (1 A cm^{-2} at 1.63 V) exhibited a much higher specific surface area than that of IrO_2 (Adams) (1 A cm^{-2} at 1.66 V), which indicated better IrO_2 dispersion.

The performance of catalysts in the OER depends strongly on the structures and morphologies.[55–61] A significant way to improve the efficiency of IrO_2 is for it to possess nanostructures with a high specific surface area. To increase the specific surface area, a porous structure (meso- or macroporous) is of great importance. To better control the pore size and degree of cross-linking, hard or soft templates with a narrow particle size distribution have been frequently employed as structure-directing agents, such as polymer microspheres (for macroporous materials) and amphiphilic block copolymers (for mesoporous materials). For example, Li et al. reported a nanoporous IrO_2 catalyst with a specific surface area of 363.3 m^2 g^{-1}, which was prepared through a facile ammonia-induced pore-forming protocol (Figures 4 and 5) with a uniform particle size and pore size distribution.[55] Micro-/mesoporous IrO_2 prepared with NH_3 exhibited an outstanding performance (10 mA cm^{-2} at 1.512 V vs. RHE) relative to that of other IrO_2 catalysts prepared without NH_3 (10 mA cm^{-2} at 1.542 V vs. RHE) and commercial IrO_2 (10 mA cm^{-2} at 1.551 V vs. RHE; 0.5 M H_2SO_4, 25 °C, *iR* correction).

Ortel et al. synthesized a mesoporous iridium oxide through soft templating and EISA, by employing an amphiphilic triblock copolymer, PEO-PB-PEO (PEO = poly(ethylene oxide), PB = poly-

Figure 4. Schematic illustration of the mechanism for the formation of nanoporous IrO_2 catalysts. Modified from Ref. [55].

© 2019 Wiley-VCH Verlag GmbH & Co. KGaA, Weinheim

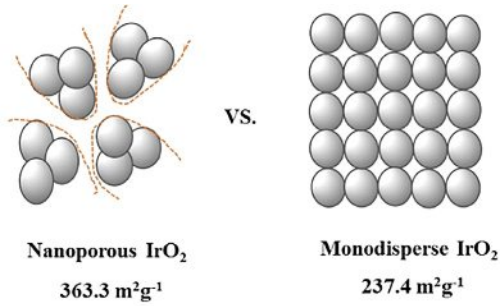

Figure 5. Specific surface areas of IrO_2 (1:100 $H_2IrCl_6/NH_3{\cdot}H_2O$ at 450 °C) and monodispersed IrO_2. Modified from Ref. [55].

butadiene).[56] The cyclic voltammogram indicated that the templated IrO_2 film exhibited significantly larger geometric current densities than that of the untemplated IrO_2 film; this can be attributed to differences in the electrochemically active surface area (ECSA) caused by differences in the coating surface morphology induced by the pore template. The overpotential for the templated mesoporous film (1.58 V vs. RHE at 100 mA cm^{-2}) is substantially lower than that for the untemplated film (1.62 V vs. RHE at 100 mA cm^{-2}) for all current densities in the OER potential region (0.1 M $HClO_4$, 25 °C, without *iR* correction). Li et al. utilized SBA-15 as a hard template to prepare mesoporous IrO_2.[57] The cell voltage of the IrO_2 (SBA-15) anode was 1.629 V at 1 A cm^{-2}, which was about 50 mV lower than that of IrO_2 obtained through the Adams protocol. In both cases, the higher activity than that of nontemplated IrO_2 has been attributed to the more uniform dispersion, larger specific surface area, and pore volume.

Iridium nanodendrites (Ir-ND) were synthesized by reducing H_2IrCl_6 with $NaBH_4$ in the presence of tetradecyltrimethyl ammonium bromide (TTAB) as an organic capping agent.[58] The highly branched structure of the iridium dendrites, with a particle size of about 10 nm, showed an enhanced OER activity. Ir-ND demonstrated the characteristics required for highly efficient catalysts, including a large specific surface area, small particle size, and a high electrochemical porosity (34.2 %) compared with that of commercial Ir blacks.[59] The rich edges and corner atoms resulting from the dendritic structure are of great importance for high catalytic activity. Kim et al. reported the highly conductive, nanoporous architectures of an Ir oxide shell on a metallic Ir core, which formed through the fast dealloying of Os from an $Ir_{25}Os_{75}$ alloy, and possessed an ideal balance between activity and stability.[62] It has been proposed that the activity–stability factor (ASF), expressed as the ratio between activity of the OER and stability of the oxides, become a new key "metric" for determining the technological relevance of oxide-based anodic water electrolyzer catalysts. The nanoporous Ir/IrO_2 morphology of dealloyed $Ir_{25}Os_{75}$ shows a factor of about 30 improvement in the ASF, relative to that of conventional Ir-based oxides, as a consequence of the nanoporous Ir oxide/Ir metal morphology, rather than through Os-induced electronic effects on Ir surface atoms. The balance between activity and stability can be addressed through the manipulation of the material morphology. ECSA itself may not be the only factor affecting the measured OER performance, and conductivity also plays a critical role in OER performance.

2.1.2. Binary, ternary, and multicomponent catalysts of iridium oxides

To reduce the IrO_2 loading, one common approach is to dope inexpensive metals, which can change the electronic and structural properties and improve the activity and stability.[63] The resulting electrocatalyst becomes a binary or ternary composite of iridium oxide with other metal oxides in the form of $Ir_xM_yN_zO_a$; M and N are inexpensive metals.

Because both RuO_2 and IrO_2 are nonstoichiometric, RuO_2 is an anoxic structure (RuO_{2-x}) and IrO_2 is a peroxy structure (IrO_{2+x}). The mixture of these two has a common effect of mutual matching. Therefore, the oxygen-evolving activity and stability of Ir and Ru binary oxides are much higher than that of single Ir or Ru. Extensive research has been performed on Ir–Ru alloys and their oxides.[64–85] Mixed oxides formed by RuO_2 and IrO_2 retain the useful properties of both components (high activity of RuO_2 and high stability of IrO_2). In Ir-rich mixed oxides, the presence of Ru increases the activity of Ir; in Ru-rich mixed oxides, the presence of Ir increases the stability of Ru. Methods to form mixed Ru–Ir oxides fall into two categories: a direct and dry film formation approach (i.e., reactive spray deposition technology)[64,65] or wet powder synthesis followed by an electrode formation step (i.e., thermal decomposition,[66,67,76] hydrolysis method,[68] Adams fusion,[42,43,69–72] or a sol–gel method).[75,80,81] The mixed oxides may be composed of homogeneous solid solutions of Ru and Ir,[64–66,70,71] or present as IrO_2 and RuO_2 separate phases.[67,68]

Along with increasing Ru content in $Ir_xRu_{1-x}O_2$, the average particle size and crystallinity of the catalysts increased. Generally, $Ir_xRu_{1-x}O_2$ compounds are observed to be more active than that of IrO_2 and more stable than that of RuO_2.[64–72] The synthetic routes have a great influence on atomic mixing, surface segregation, and particle size. XRD and ICP atomic emission spectroscopy (AES) measurements by Mayousse et al. highlighted that the quantity of Ru inserted into the oxide lattice, through the Adams fusion method, could be finely controlled without any phase separation.[43] Siracusano et al. applied a preleaching procedure to achieve a high degree of surface purity and promote an enrichment of Ir on the outer surface.[72] The Ir content in the Ru-based catalyst composition contributes to its stability against dissolution, without increasing the overpotential at its surface. Cheng et al. observed that RuO_2 as an anodic electrocatalyst was unstable, with the potential rising to 8 V versus a standard calomel electrode (SCE) at about 20 000 s. $Ir_{0.2}Ru_{0.8}O_2$ shows a higher stability than that of RuO_2, and the potential is lower than 2 V versus SCE, even as the time approaches 40 000 s.[70] An increase in performance has been well documented upon Ru insertion.[67] Felix et al. further proved that the addition of RuO_2 to IrO_2 improved the activity for the OER.[71] $Ir_{0.7}Ru_{0.3}O_2$, although displaying a slightly lower activity than that of $Ir_{0.9}Sn_{0.1}O_2$, is claimed to be the most promising electrocatalyst for the OER because no decrease in activity occurs as the RuO_2 content is increased to 30 mol %.

© 2019 Wiley-VCH Verlag GmbH & Co. KGaA, Weinheim

Hence, the interaction of Ir–Ru and the synergetic contribution to the activity are of great interest.

Core–shell nanocatalysts have been widely studied over the past decades in catalysis, biology, and energy storage. The activity and catalytic efficiency are directly influenced by the surface composition and stability of the nanocatalysts. For example, Ma et al.[86] employed carbon-supported ruthenium as the template to prepare RuO_2@IrO_2 core–shell nanocatalysts, and the OER specific activity of RuO_2@IrO_2 (5.5 $\mu A\,cm^{-2}{}_{ox}$) was threefold greater than that of IrO_2 (1.7 $\mu A\,cm^{-2}{}_{ox}$) at 1.48 V versus RHE in a 0.5 M solution of H_2SO_4. Li et al. developed the discontinuously covered IrO_2–RuO_2@Ru (the Ir/Ru ratio changes from 1:1 to 3:1) supported structure. IrO_2–RuO_2@Ru (3:1) exhibits the most uniform NP distribution and the highest activity among all catalysts, showing an overpotential of only 281 mV at 10 $mA\,cm^{-2}$.[87] Meanwhile, excellent durability has been achieved, with the overpotential positively shifting by only 16 mV at 10 $mA\,cm^{-2}$ after 3000 cycles through accelerated durability tests (ADTs). Audichon et al. synthesized a core–shell-like IrO_2@RuO_2 material using a surface modification/precipitation route in an ethanol medium. The crystalline RuO_2 core particles are well covered by IrO_2.[88] Compared with pure IrO_2 or pure RuO_2, IrO_2@RuO_2 displayed the highest accessibility of active sites and showed the most promising activity for the OER, owing to intimate contact between the two oxides in the IrO_2-covered RuO_2 nanocatalysts, which combined the intrinsic activity of RuO_2 and the stability of IrO_2.[88] Danilovic et al. found that the Ru–Ir system employed the power of surface segregation to form a nanosegregated "Ir-protective skeleton" that was four times more stable, but equally as active as commercially available Ru–Ir alloy anode catalysts.[82] The activity of oxide materials for the OER is primarily controlled by the stability of surface atoms, rather than the energy of adsorption of reaction intermediates.

To improve the active surface area of $Ir_xRu_{1-x}O_2$, the synthesis of $Ir_xRu_{1-x}O_2$–MO_x (M = Sn, Ta, Mo, Co, Ce, Pt as the dopant metal) is an effective way,[90–100] and nonprecious metal oxides are added to noble-metal mixed oxides. For example, Hutchings et al. demonstrated that a ternary mixed oxide containing SnO_2, RuO_2, and IrO_2 was more stable than catalysts consisting of noble-metal oxides only.[90] $Ir_{0.25}Ru_{0.25}Sn_{0.5}O_2$ showed an initially lower activity, but a significantly improved stability, which resulted in a superior behavior to that of IrO_2 and $Ru_{0.5}Ir_{0.5}O_2$ for testing times of 320 and 730 h. Ir–Ru–Sn ternary oxide coated electrodes fabricated by thermal decomposition revealed the synergistic/antagonistic effects between the mixed oxides. Marshall et al. synthesized oxide powders of $Ir_xRu_yTa_zO_2$ by means of aqueous hydrolysis, followed by thermal oxidation.[91] A remarkable performance has been obtained by using anode materials containing 20–40 mol% Ru and 0–20 mol% Ta. The doped MO_x often has weak catalytic activity and conductivity; a high proportion of dopant has proven to be unavailable.[91–95] Thus, the doped content in $Ir_xRu_{1-x}O_2$–MO_x must be achieved in a highly controlled manner. $Ir_{0.4}Ru_{0.6}Mo_xO_y$ prepared by means of a modified Adams fusion method had a decreased particle size and improved BET surface area, without deterioration of the conductivity.[96] Iridium and ruthenium ions at the interface can connect with molybdenum through Ir(Ru)–O–Mo bonds around the rutile crystallite, which inhibits the growth of crystallite grains during the fusion process. A single cell with $Ir_{0.4}Ru_{0.6}Mo_xO_y$ (1 $A\,cm^{-2}$ at 1.646 V) shows a higher performance than that of a cell with $Ir_{0.4}Ru_{0.6}O_2$ (1 $A\,cm^{-2}$ at 1.606 V) under the conditions without *IR* correction. The $RuIrCoO_x$ powders were synthesized through a chemical reduction method, followed by thermal oxidation.[97] A single cell with $RuIrCoO_x$ showed a higher performance than that of a cell with $IrRuO_x$. The cell voltages at 30 $mA\,cm^{-2}$ are 1.80 and 1.88 V for $RuIrCoO_x$ and $IrRuO_x$, respectively.

In recent years, mixed oxides formed by dispersing the noble-metal oxide in a more stable nonprecious matrix have been intensively investigated. For instance, binary IrO_2–SnO_2 catalysts are of interest because of the elevated conductivity and stability at high temperatures[47,75,96–112] IrO_2–SnO_2 has been prepared by means of Adams fusion,[43,71,92] sol–gel,[101,104] modified polyol,[92,93] reactive cosputtering,[113] and surfactant-assisted methods.[102] The crystalline properties of $Ir_xSn_{1-x}O_2$ powders depend on the method used to prepare such materials. The Adams fusion method resulted in oxides consisting of at least two separate oxide phases, namely, a Sn-rich oxide and an Ir-rich oxide.[92] In contrast to commercial Ir black, $Ir_xSn_{1-x}O_2$ ($x = 1$, 0.67, and 0.52) NPs developed by means of a surfactant-assisted method are amorphous, with good dispersion, high pore volume, a solid-solution state, and an Ir-rich surface for bimetal oxides.[102] Mayousse et al. performed XRD and ICP-AES measurements to highlight that the quantity of tin was inserted into the oxide lattice in a finely controlled manner.[43] The bulk molar fraction of Sn was introduced into the IrO_2 lattice without phase separation. The crystallinity increased with the addition of SnO_2.[71] Similar crystal structure and lattice parameters of IrO_2 and SnO_2, and comparable ionic radii of Ir^{4+} (0.077 nm) and Sn^{4+} (0.083 nm), allow the formation a tetragonal $Sn_xIr_{1-x}O_2$ solid solution. A solid solution between iridium and tin oxides with lattice parameters of the solid-solution phase showed a linear relationship over the entire composition range.[92,93,104] For example, Ardizzone et al. showed that iridium could substitute tin in the lattice at any temperature, and the composites obtained at 500 °C produced the highest stability thanks to their ordered structures.[101] The effect of tin addition to iridium on the performance of the OER is controversial. Marshall et al. proved that the electrical resistivity increased as tin was added to the oxide.[92,93] There is a significant difference between the materials produced by means of Adams fusion and the modified polyol method. The former shows twice as high electrical resistivity as that of the latter, owing to the difference in structure of the oxides. A lower resistivity could be expected in a solid solution due to a continuous electronic path through the oxides. The insulating tin oxide phase in two-phase oxide powders reduced the electronic pathway.[92] The addition of tin oxide to iridium oxide particles shows no beneficial effect other than the dilution of more expensive iridium oxide. Pure IrO_2 anodes have the best performance (1.61 V) at 1 $A\,cm^{-2}$ and 90 °C.[93] The active area or the number of active sites decreases as the tin content increases. Felix et al. showed that $Ir_xSn_{1-x}O_2$ (Sn = 10 mol%) had a significant in-

© 2019 Wiley-VCH Verlag GmbH & Co. KGaA, Weinheim

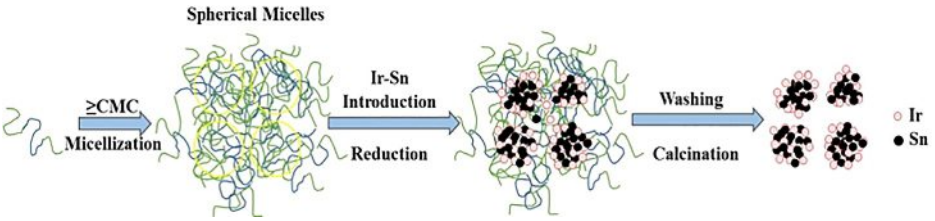

Figure 6. Schematic illustration of the surfactant-assisted method for the fabrication of $Ir_xSn_{1-x}O_2$ ($0<x<1$) NPs with a high Ir content. CMC = critical micelle concentration. Modified from Ref. [102].

crease in electrocatalytic activity compared with that of pure IrO_2.[71] Li et al. showed that the structure of the resulting $Ir_xSn_{1-x}O_2$ samples was strongly related to the Ir/Sn composites.[102] Figure 6 illustrates the strategy of the surfactant-assisted method for the synthesis of $Ir_xSn_{1-x}O_2$ ($0<x<1$) NPs with high Ir contents. $Ir_xSn_{1-x}O_2$ ($x=0.67$, 0.52) NPs displayed outstanding activity and stability, owing to the amorphous structure, good dispersion, high pore volume, solid-solution state and Ir-rich surface, relatively large size (10–11 nm), and dissolution of the Sn component (Figure 7). The membrane electrode assembly (MEA) performance with $Ir_{0.52}Sn_{0.48}O_2$ as the anode showed a better performance for 1 A cm^{-2} at 1.631 V and 2 A cm^{-2} at 1.821 V. Xu et al. observed that at low SnO_2 contents the IrO_2 particles were well dispersed, but at higher SnO_2 contents the active surface area of IrO_2 decreased due to an increase in the average particle size.[103]

Ternary Ir–Sn-based mixed oxides have been extensively evaluated as the OER anode electrocatalysts. Pérez-Viramontes et al. prepared the Ir–Sn–Sb–O through a conventional thermal decomposition method.[110] According to the onset potential for the OER tested in 0.5 M H_2SO_4, the Ir–Sn–Sb–O (40 at% Ir) (1.39 V vs. RHE) electrodes demonstrated a higher activity than that of the IrO_2/CV (1.45 V vs. RHE; CV = cyclic voltammetry) and IrO_2/ATO (1.52 V vs. RHE). The OER kinetics has been improved for the Ir–Sn–Sb–O materials with respect to the mechanical mixture of IrO_2/ATO. The Ir–Sn–Sb–O electrode was also more stable towards the OER at an applied potential of 1.55 V versus RHE than that of IrO_2 supported on Vulcan carbon. Ternary Sn–Ir–Ta systems have been synthesized through a controlled sol–gel method.[111] In comparison with SnO_2 and binary SnO_2–IrO_2 materials, ternary mixtures presented higher catalytic activities because Ta increased the surface area, improved the electronic conductance and charge-storage capacitance, and promoted the surface enrichment of Ir. Kadakia et al. synthesized $Ir_{1-2x}Sn_xNb_xO_2$ through thermal decomposition and coated the product on Ti foil.[112] The activity of $Ir_{0.40}Sn_{0.30}Nb_{0.30}O_2$ was similar to that of pure IrO_2, with about 60 mol% reduction in noble-metal content, whereas $Ir_{0.20}Sn_{0.40}Nb_{0.40}O_2$ was only 20% lower than that of pure IrO_2, with about 80 mol% reduction in noble-metal content, which achieved a remarkable reduction in noble-metal oxide loading. Xu et al. first synthesized Pt-activated IrO_2/SnO_2 (2 A cm^{-2} at 1.63 V) nanocatalysts for the OER; these catalysts showed an enhanced activity relative to that of IrO_2/SnO_2 (2 A cm^{-2} at 1.66 V).[114] This was attributed to the cooperative effects of improved electrical conductivity and the synergistic effect of Pt and IrO_2/SnO_2, whereas Pt–IrO_2/SnO_2 showed short-term stability at 1.52 V and 80 °C in a laboratory-scale single-cell setup.

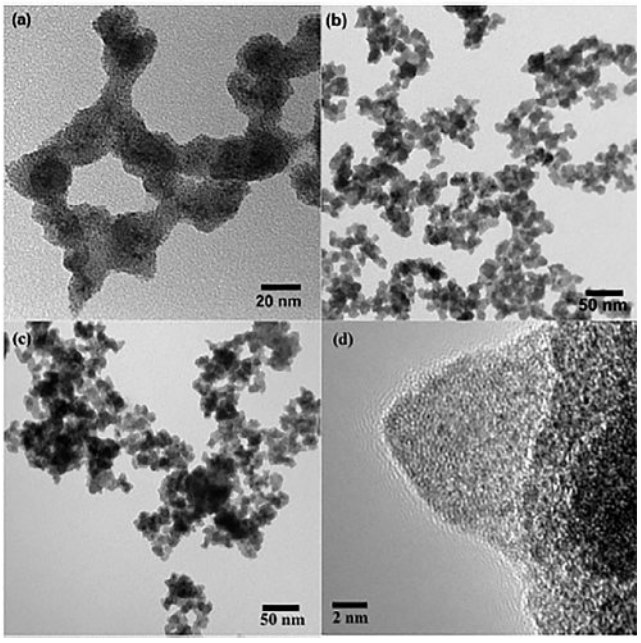

Figure 7. TEM images of a) as-synthesized $Ir_{0.67}Sn_{0.33}O_2$, b) IrO_2, and c) $Ir_{0.67}Sn_{0.33}O_2$, and d) a high-resolution (HR)TEM image of $Ir_{0.67}Sn_{0.33}O_2$. Reproduced with permission from Ref. [102]. Copyright The Owner Societies 2013.

To improve the catalytic activity, a novel dopant/alloying element (F^-) is added to the noble-metal oxide electrocatalyst (e.g., IrO_2 or RuO_2). A fluorine-doped IrO_2 thin film has been studied as a promising oxygen evolution anode electrocatalyst that exhibits a significant improvement in catalytic activity compared with that of pure IrO_2.[115–121] Kadakia et al. synthesized fluorine-doped IrO_2 through thermal decomposition of a homogeneous mixture of $IrCl_4$ and NH_4F dissolved in ethanol/deionized water that was solution coated onto pretreated Ti foil, ranging from 0 to 30 wt% F.[115,116] Thin-film IrO_2:F with 20 wt% F ($(\approx 11.6 \pm 0.1)$ mA cm^{-2} at 1.65 V vs. NHE) showed about 19% higher catalytic activity than that of pure undoped IrO_2 (≈ 9.4 mA cm^{-2} at 1.65 V vs. NHE) in a 1 N solution of H_2SO_4 at 40 °C, which suggested that F-doped IrO_2 could be a promising anode catalyst for the OER. They also synthesized (IrO_2:F) powders with varying F contents, ranging from 0 to 20 wt%, by using a modified Adams fusion method.[117] The IrO_2:F sample with an optimum composition of IrO_2:10 wt% F

© 2019 Wiley-VCH Verlag GmbH & Co. KGaA, Weinheim

showed remarkably superior activity and stability relative to that of pure IrO_2. IrO_2:F is a solid solution of a single rutile tetragonal structure without any undesirable phase formation, such as pure IrO_2. This might be due to the similar ionic radii of O^{2-} and F^- (125 and 120 pm, respectively). The molar volume of IrO_2:F with different compositions is comparable to that of pure IrO_2, which indicates that F^- doping, instead of O^{2-}, has no significant effect on the molar volume of IrO_2:F.

To improve the electrical conductivity of SnO_2, Datta et al. studied F-doped SnO_2, which had a high corrosion resistance and was electrically conductive. (Sn,Ir)O_2:F containing 10 wt% F showed the same electrochemical activity as that of IrO_2 ($(\approx 14 \pm 1)$ mA cm^{-2} at 1.55 V vs. NHE, 40 °C, 1 N H_2SO_4, after iR_Ω correction) with about 80 mol% reduction in IrO_2.[118,119] $Ir_{0.3}Sn_{0.35}Nb_{0.35}O_2$:10 wt% F proved to be a promising anode electrocatalyst, resulting in about 70 mol% reduction in IrO_2 content without any compromise in activity, and the current density of $Ir_{0.3}Sn_{0.35}Nb_{0.35}O_2$:10 wt% F at 1.55 V ($\approx$16 mA cm^{-2} at 1.55 V vs. NHE) was slightly higher than that of pure IrO_2 ($\approx$12 mA cm^{-2} at 1.55 V vs. NHE; 40 °C, 1 N H_2SO_4, after iR_Ω correction).[120] All of them formed a single-phase, homogeneous solid solution without any undesirable phase separation. The molar volumes of IrO_2:F, (Sn,Ir)O_2:F, and (Ir,Sn,Nb)O_2:x wt% F are comparable to those of pure IrO_2, (Sn,Ir)O_2, and (Ir,Sn,Nb)O_2, respectively; thus indicating that F^- ion substitution/doping has no significant effect on the overall molar volume. This might be due to the comparable ionic radii of O^{2-} (125 pm) and F^- (120 pm). The excellent activity exhibited by F-doped IrO_2, along with its long-term stability, make it an appealing anode electrocatalyst for the OER in SPE-based water electrolysis.

Another approach involved mixing of platinum-group metals (PGMs; Pt[122–124] and Rh[125]) with IrO_2. These PGM oxides are very stable under acidic conditions and very conductive. For example, Ye et al. prepared a novel Ti/Pt–IrO_2 electrocatalyst by using the dip-coating/calcination method, in which Pt served as a dispersing agent and IrO_2 served as a catalyst.[123] The incorporation of Pt into IrO_2 not only increased the conductivity, but also resulted in a synergic effect to make Pt–IrO_2 much more stable. Seley et al. found that the addition of Rh appeared to stabilize and/or enhance the OER activity of IrO_2.[125] Other less expensive and highly corrosion-resistant metal oxides, including Nb_2O_5,[126–128] Ta_2O_5,[69,71] and SnO_2, have been explored as alternative anode candidates for SPE water electrolysis; these would improve the overall corrosion characteristics of noble-metal oxide electrocatalysts and reduce the cost of noble-metal loading. Felix et al. synthesized $Ir_xTa_{x-1}O_2$ ($1 \geq x \geq 0.7$) by adapting the Adams fusion method.[71] The addition of Ta_2O_5 to IrO_2 improved the activity, for example, $Ir_{0.8}Ta_{0.2}O_x$ ($\approx$55 mA cm^{-2} at 1.6 V vs. 3 M Ag/AgCl electrode) and pure IrO_2 ($\approx$35 mA cm^{-2} at 1.6 V vs. 3 M Ag/AgCl electrode) (0.5 M H_2SO_4, 25 °C), and suppressed crystal growth.

2.1.3. Supported catalysts

To reduce the cost of the catalyst and to enhance the electrocatalytic activity and life span, one solution is to support electrocatalytic NPs on high specific surface area materials, which will reduce agglomeration of the electrocatalyst and increase the active surface area. Due to the high overpotential and corrosive nature of the OER environment, the presence of carbon in the active layer leads to the oxidation of supporting substrate [Eq. (3); at 0.206 V vs. a standard hydrogen electrode (SHE)], which is not suitable as a support for the OER under acidic conditions.

$$C + 2\,H_2O \rightarrow CO_2 + 4\,H^+ + 4\,e^- \quad (3)$$

The requirements for a suitable support of the OER electrocatalyst include 1) high availability and low cost, 2) high stability in an acidic environment, 3) high specific surface area, and 4) good electrical conductivity. The enhanced activity is related to the interaction between the support and electrocatalyst. Various materials have been applied as supports of Ir, including metal oxides, such as ATO,[129–144] TiO_2,[145–158] titanium suboxide (Ti_nO_{2n-1}),[159–161] or ITO,[166,167] and carbides, such as TiC,[168,169] TaC,[170,172] SiC,[173] or WC,[174–176] due to their corrosion resistance and electrical conductivity.

Thanks to its good electronic conductivity, availability, high specific surface area, and stability at anodic potentials, ATO has been widely used as a support for the OER.[129–144] The performance of ATO-supported Pt or RuO_2 was better than that of pristine Pt/C or RuO_2.[129,130] The Pt/ATO catalyst possessed about 90% of the original catalytic activity after 3000 cycles, whereas Pt/C retained about 36% activity. With the same amount of RuO_2, RuO_2/ATO exhibited a higher voltammetric charge than that of unsupported RuO_2. This was attributed to the lower agglomeration of active crystallites on ATO. The effects of various parameters, such as particle size, electronic conductivity, and specific surface area, on the performance of the ATO-supported IrO_2 catalysts were systematically investigated. Marshall and Haverkamp studied a bimetallic IrO_2–RuO_2 catalyst supported on commercial ATO NPs with various loading levels (5, 10, and 20 wt%).[131] The ECSA of 75 mol% IrO_2/25 mol% RuO_2 clusters is maximal, but the ECSA decreased with decreasing loading of IrO_2–RuO_2 on ATO, and 20 wt% $Ru_{0.25}Ir0_{.75}O_2$ on ATO presented the highest activity in a 0.5 M aqueous solution of H_2SO_4. Puthiyapura et al. achieved 40 wt% reduction in IrO_2 by utilizing ATO as a support material.[133] The MEA performance was better for 60 wt% IrO_2/ATO (1625 mA cm^{-2} at 1.8 V) than that of pristine IrO_2 (1341 mA cm^{-2} at 1.8 V) under the same conditions in which the MEA involved Nafion-115 membrane at 80 °C and atmospheric pressure. The higher performance of 60 wt% IrO_2/ATO was mainly attributed to a better dispersion of active IrO_2 on the electrochemically inactive ATO support materials, the smaller IrO_2 crystallites formed, a continuous electronic network, a higher BET surface area, and similar conductivity to that of pristine IrO_2. Previous research from Strasser and co-workers[59,134–137] studied mesoporous Sb-doped tin oxides synthesized through a tetradecylamine (TDA) soft-template method as supports, and found that these supports were highly stable, relative to carbon black, due to their mesoporous structure, small particle size, high specific surface area, and electrical con-

© 2019 Wiley-VCH Verlag GmbH & Co. KGaA, Weinheim

ductivity. The Ir-ND/ATO catalyst displayed more than twofold higher kinetic water-splitting activity compared with that of IrO_x/C, and eightfold greater catalytic mass-based activity than that of commercial Ir black.[59] The metal/metal oxide–support interactions (MMOSI) play a critical role in the performance of Ir acidic water-splitting catalysts.[137] At a higher current density of 10 mA cm^{-2}, the measured potential sharply increased to 2.4 V (vs. RHE) after 15 min and 1.2 h for IrO_x/C (Vulcan XC-72R, Cabot, 235 m^2 g^{-1}) and IrO_x/Com. ATO (commercial ATO, SnO_2/Sb_2O, ≥99.5%, Sigma–Aldrich, 47 m^2 g^{-1}), respectively, whereas the IrO_x/ATO catalyst showed a negligible degradation during the stability test, although their working potentials were initially similar. After the stability test, the Ir mass loss of IrO_x/ATO was 28.3% of the initial Ir loading, whereas that of IrO_x/C was 97.1%, which suggested that the MMOSIs helped to maintain a higher IrO_x loading, and thus, sustained higher charge-transfer kinetics. The Meso-ATO powder has a higher specific surface area (264 m^2 g^{-1}) than that of Com. ATO. Nong et al. presented a novel catalyst/support couple concept—an electrochemically dealloyed IrNi core–IrO_x shell concept combined with a mesoporous corrosion-resistant oxide support.[136] The $IrNiO_x$ core–shell structure has been obtained from IrNi NP precursor alloys through the electrochemically selective dealloying of Ni and simultaneous surface oxidation of the surface Ir atoms, resulting in IrO_x shells. $IrNiO_x$/Meso-ATO core–shell material (≈90 A g$^{-1}_{Ir}$) showed 2.5 times higher Ir-mass-based activity than that of IrO_x/C (Vulcan XC-72R, ≈250 m^2 g^{-1}; ≈40 A g$^{-1}_{Ir}$) and IrOx/Com. ATO (Sigma Aldrich, 47 m^2 g^{-1}; ≈35 A g$^{-1}_{Ir}$) at an overpotential of $\eta = 280$ mV versus RHE in 0.05 M H_2SO_4. Figure 8 illustrates the structure hypothesis regarding the active catalyst/support couple. With thin IrO_x shells on the Ir-low/Ir-free cores, the proceeding OER reduced the amount of Ir significantly. Wang et al. prepared a novel OER catalyst composed of Ir supported on a SnO_2:Sb aerogel (Ir/SnO_2:Sb-mod-V), which allowed a decrease in precious-metal usage of more than 70 wt% in the catalyst layer, while maintaining a similar OER activity to that of its unsupported counterpart.[141]

TiO_2 is an option because of its high resistance against anodic corrosion and controllable morphology. Because TiO_2 itself typically shows insulating properties, electrocatalysts must be introduced into TiO_2 by coating or doping. For example, Mazúr et al. studied the electrocatalysts IrO_2/TiO_2 with three TiO_2 samples, namely, R200M (10 m^2 g^{-1}), P25 (50 m^2 g^{-1}), and P90 (90 m^2 g^{-1}), at different specific surface areas.[145] A lower specific surface area of the TiO_2 support results in a higher activity of the catalyst, due to the formation of a conductive IrO_2 film on the surface of nonconductive supports. Oakton et al. developed a high specific surface area IrO_2–TiO_2 catalyst that was chlorine free, which was a highly active and stable OER catalyst in acidic media.[146] The 40 mol% IrO_2–TiO_2 catalyst improved the OER activity and stability compared with that of the benchmark catalyst. The presence of iridium hydroxo surface species was associated with high OER activity. Lu et al. revealed that IrO_2/H-TNTA reached a fivefold higher current density at 1.6 V versus RHE in 0.5 M H_2SO_4 than that of IrO_2/air-TNTA with improved conductivity.[147] Conductive suboxides of titanium, such as Ebonex, have been studied as electroactive materials. Siracusano et al. prepared titanium suboxides with a Magnéli phase as the conductive supports of IrO_2.[159] As a result, IrO_2 based on Ti suboxides exhibited a larger voltammetric charge and double-layer capacitance than that of the anode based on the commercial support, owing to a better dispersion and larger occurrence of active catalytic sites on the surface of the suboxide.[160,161] TiO_2 doped with Nb[162–164] and V[165] has been reported to achieve considerable conductivity and high stability. Hao et al. found that IrO_2/TN-20 (20 at% Nb) possessed the highest OER activity (2.027 V at 1 A cm^{-2}) and was superior to that of pristine IrO_2/TiO_2 (2.218 V at 1 A cm^{-2}) in single-cell tests at 80 °C.[162] The increase in OER activity originated from Nb doping, which restricted the crystal structure to a single phase of anatase and induced an enhancement of the specific surface area and activity of transferring charge and species. The additional redox couples of Nb^{IV}/Nb^{V} accounted for this enhancement. Xia et al. studied IrO_2/$Nb_{0.05}Ti_{0.95}O_2$ (26 wt%) and revealed the best mass-based activity at 1.6 V versus RHE (471 A g^{-1} IrO_2^{-1}) in 0.5 M H_2SO_4;[163] this was 2.4-fold larger than that of unsupported IrO_2 (198 A g^{-1} IrO_2^{-1}). Hao et al. found that 40Ir/TV-20 (titania doped with 20 at% V) emerged as the best V-doped titania support for the IrO_2 catalyst (2.015 V at 1 A cm^{-2}, 80 °C).[165] The V dopant on titania supports enhanced the simplification of the phase composition, and consequently, improved the homogeneity of the porous morphology, and introduced the V^{IV}/V^{V} redox couple to the surface of titania. Other materials, such as ITO,[166,167] TiC,[51,168,169] TaC,[170,172] Ta_2O_5,[171] WC, WO_3,[174–176] and reduced graphene oxide (RGO),[177] were also studied as support materials for anode catalysts. Puthiyapura et al. picked ITO as a support because of the remarkable thermal stability of ITO.[166] The 90% IrO_2-ITO catalyst produced a similar performance (1.74 V at 1 A cm^{-2}) to that of unsupported IrO_2 (1.73 V at 1 A cm^{-2}) under the same working conditions (MEA polarization test at 80 °C with Nafion 115 membrane). Kúš et al. prepared a thin Ir film on a TiC-based support sublayer through magnetron sputtering.[51] The supported Ir/TiC catalysts had a higher stability than that of pristine Ir, which was in good agreement with the findings by Sui et al.[168,169] WC and WO_3 have been chosen as supports,[174] and the optimal route to WO_3/WC-supported $Ir_{0.5}Ru_{0.5}O_2$ catalysts was mechanical mixing of support and cat-

Figure 8. Schematic illustration of the OER on the IrO_x shell of $IrNiO_x$ core–shell NPs supported on Meso-ATO. Modified from Ref. [136].

© 2019 Wiley-VCH Verlag GmbH & Co. KGaA, Weinheim

alyst followed by annealing under an inert atmosphere. Kong et al.[177] proved that the catalytic activity of the IrO_2/RGO (1.65 V vs. RHE at 5.01 A mg^{-1}) hybrid towards the OER was 2.3 times that of commercial IrO_2 (1.65 V vs. RHE at 2.19 A mg^{-1}) in the OER polarization curves in 0.5 M H_2SO_4 at 25 °C. These results were attributed to a better dispersion of active IrO_2 on the electrochemically inactive support, giving rise to smaller catalyst particles, and thereby, a higher specific surface area. All supported catalysts showed a higher efficiency of utilization of the precious metal than that of pure IrO_2, suggesting that these oxides may be of economic advantage to use as SPE water electrolysis anodes.

2.1.4. Structural modification of iridium oxides

NP materials efficiently dispersed on support, highly porous layered, core–shell, and mixed oxide systems have been suggested to reduce the loading of expensive elements. An alternative way is to structurally modify iridium oxides. Extensive efforts have been devoted to resolving the structure–property relationship.[178–194]

Recent development of techniques for the high-quality growth of epitaxial complex oxide thin films and heterostructures provides an intriguing opportunity for the conception and fundamental study of OER catalysts.[178,179] For example, Saveleva et al. developed a nanostructured iridium catalyst after electrochemically leaching ruthenium from metallic iridium–ruthenium,[178] that is, $Ir_{0.7}Ru_{0.3}O_x$ (EC). The dissolution of unstable Ru led to an unparalleled OER activity of the remaining Ir-rich catalyst compared with that of classic thermally treated $Ir_{0.7}Ru_{0.3}O_2$ (TT). $Ir_{0.7}Ru_{0.3}O_x$ (EC) (1.68 V at 1 A cm^{-2}) showed an unparalleled 13-fold higher OER activity relative to that of $Ir_{0.7}Ru_{0.3}O_2$ (TT) (1.73 V at 1 A cm^{-2}); thus proving that $Ir_{0.7}Ru_{0.3}O_x$ (EC) was one of the most efficient anodes, to date. Seitz et al. reported an iridium oxide/strontium iridium oxide (IrO_x/$SrIrO_3$) catalyst that was formed during electrochemical testing by strontium leaching from surface layers of thin films of $SrIrO_3$.[179] The IrO_x/$SrIrO_3$ catalyst outperformed well-known IrO_x and RuO_x systems. DFT calculations suggested the formation of highly active surface layers during strontium leaching with IrO_3 or anatase IrO_2 motifs. Surface IrO_x formed by means of the in situ leaching of Sr from $SrIrO_3$, which was more active than that of deposited IrO_x. Figure 9 shows AFM maps and line scans for a 100 nm $SrIrO_3$ film before and after OER testing for 30 h. Although there was some surface rearrangement, the films exhibited uniform, small features after stability testing. The stability and high intrinsic activity of this catalyst are promising for its integration into renewable energy technologies, such as PEM electrolyzers, for the sustainable production of hydrogen or other fuels and chemicals.

In addition, the most prominent examples are iridium-based perovskites, which have recently been investigated in acidic electrolyte.[179–184] Grimaud et al. used La_2LiIrO_6 as a model catalyst because the OER activity for Ir- or Ru-based oxides is often associated with surface instability.[183] This correlation is rooted in the activation of surface oxygen, leading to the modification of iridium coordination. Perovskites show high dissolution in

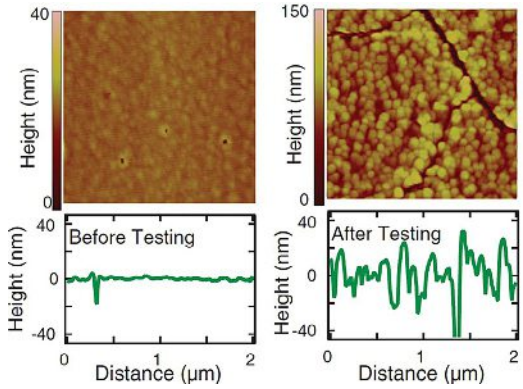

Figure 9. AFM maps and line scans for a 100 nm $SrIrO_3$ film before and after OER testing for 30 h. Reproduced with permission from Ref. [179]. Copyright The http://sciencemag.org Science 2016.

the range of amorphous/hydrous oxide, and therefore, might not be suitable for long-term operation. Similar structures can be achieved by leaching Sr from $SrIrO_3$ or Ni from $IrNiO_x$.[179,181] A case study on iridium-based perovskites showed that leaching of the non-noble elements from mixed oxides resulted in the formation of highly active amorphous iridium oxide, the instability of which was explained by the generation of short-lived vacancies that favored dissolution. The participation of activated lattice oxygen atoms triggered enhanced activity and the high dissolution rate was due to oxygen vacancies. Activity is not related to the chosen rare-earth element, but rather to the amorphous structure that forms after leaching. These insights inspired further research to be devoted to increasing the utilization of highly durable pure crystalline iridium oxide and finding solutions to stabilize amorphous iridium oxides.

Iridium, among other metals, is able to form an amorphous hydrous oxide under continuous potential cycling. In these studies,[185–187] the key role of amorphous iridium oxohydroxides in high current, stable, OER electrocatalysis is highlighted, in contrast to that of less active crystalline IrO_2. Pfeifer et al. investigated the electronic structure of active iridium oxide based catalysts and confirmed the higher OER performance of amorphous iridium(III/IV) oxohydroxides in comparison with that of IrO_2.[189,190] The superior intrinsic activity of these materials was relevant to the ability to accommodate nucleophilic reactive oxygen species.[191] Willinger et al. concluded that the ratio between corner- and edge-sharing IrO_6 octahedra determined the OER activity.[193] Thus, a high number of corner-sharing oxygen atoms (activated oxygen) facilitates the OER. They also identified key hollandite-like structural motifs associated with high catalytic activity and stability in the OER. Massué et al. synthesized novel iridium oxohydroxides through a rapid microwave-assisted hydrothermal procedure, which bridged the gap between electrodeposited amorphous IrO_x films and crystalline IrO_2 electrocatalysts prepared through calcination routes.[194] In addition, the K^+ cation has a great influence on the performance of the catalyst. The residual presence of K ions in the IrO_x-FHI (IrO_x hydroxide synthesized at the Department of Inorganic Chemistry of the Fritz Haber Institute) catalyst might play an important role in catalytic stability because

© 2019 Wiley-VCH Verlag GmbH & Co. KGaA, Weinheim

it stabilizes the hollandite-like open framework structure.[193] K^+ cations present in smaller amounts in the iridium oxohydroxides obtained for KOH/Ir (5:1) play a major role in stabilizing a high-performance iridium oxohydroxide phase containing high amounts of OER-relevant hydroxyl groups. These studies provided several important clues for the structural features that determined the OER performance of iridium oxohydroxides.[194,195]

3. Conclusions and Perspectives

Water is the most renewable resource available for sustainable hydrogen production in the future. Water electrolysis is an important production method, and based on this technology, hydrogen with a high purity of up to 99.999 vol% can be obtained upon drying and removal of oxygen impurities. SPE water electrolysis has more advantages, including small size and mass, low gas crossover and power consumption, high proton conductivity, high pressure operation, and greater safety, than those of traditional alkaline water electrolysis. For SPE electrolyzers, the current efficiency has reached as high as 99%. The main disadvantage of SPE water electrolysis is slow kinetics, which is one of the largest sources of cell efficiency loss for the OER. The development of active and stable OER catalysts has been extensively investigated.[89] The material composition and morphology have an impact on the catalyst activity toward the OER and corrosion stability. With increasing temperature, the crystallite size and crystallinity increase, the crystal specific surface area decreases, and the electrocatalytic activity decreases.

There are two main strategies to improve the activity of an electrocatalyst. One is to increase the number of active sites on a given electrode, such as through alloying or doping inexpensive metals into the iridium catalyst or by supporting NPs on high surface area materials, which can change the electronic and structural properties and improve the activity and stability. Supported catalysts can significantly increase the dispersion of the active phase, providing a high specific surface area and sufficient active sites for the OER. The other method is to increase the intrinsic activity of each active site, which can be achieved through the introduction of defects.

Many studies have been conducted on methods and materials for the anodes of SPE water electrolysis, but the situation remains challenging. To date, no credible alternative to IrO_2 has been reported. Hence, substantial research and development efforts are needed to elucidate the details of the electrode–electrolyte interface in theory and experiments. The development of both experimental and computational methods is an important frontier that can precisely unravel the reaction mechanisms on catalyst materials and under harsh operating conditions. An appropriate theoretical model incorporating the kinetics at the surfaces of the electrode and transport in the membrane should be established to analyze the current–potential characteristics of a SPE water electrolysis cell based on the involved charge and mass balances. This useful information will pave the way for the development of high activity and stability of OER catalysts.

Acknowledgements

Financial support was provided by the National Natural Science Foundation of China (project nos. 51503187, 21504037, and 51603194); the National Key R&D Project (project nos. 2016YFE0102700); the Shanxi Provincial Foundation for Science and Technology Research (project nos. 201601D021058, 201701D221050, 20181101006, and 20181102019). Partial support is also from NIMHD-RCMI grant number 5G12MD007595 from the National Institute of Minority Health, Health Disparities and NIGMS-BUILD grant number 8UL1GM118967 and the National Science Foundation (grant 1700429). Q.G. was supported as part of the Fluid Interface Reactions, Structures and Transport (FIRST) Center, an Energy Frontier Research Center funded by the U.S. Department of Energy, Office of Science, Office of Basic Energy Sciences. A portion of this work was conducted at the Center for Nanophase Materials Sciences, which is a DOE Office of Science User Facility. This manuscript has been authored by UT-Battelle, LLC, under contract no. DE-AC0500OR22725 with the U.S. Department of Energy. The United States Government retains and the publisher, by accepting the article for publication, acknowledges that the United States Government retains a nonexclusive, paid-up, irrevocable, worldwide license to publish or reproduce the published form of this manuscript, or allow others to do so, for the United States Government purposes. The Department of Energy will provide public access to these results of federally sponsored research in accordance with the DOE Public Access Plan (http://energy.gov/downloads/doe-public-access-plan).

Conflict of interest

The authors declare no conflict of interest.

Keywords: electrochemistry · iridium · solid polymer electrolytes · supported catalysts · water splitting

[1] Z. W. Seh, J. Kibsgaard, C. F. Dickens, I. Chorkendorff, J. K. Nørskov, T. F. Jaramillo, *Science* **2017**, *355*, eaad4998.
[2] N. S. Lewis, *Science* **2016**, *351*, aad1920.
[3] F. Barbir, *Sol. Energy* **2005**, *78*, 661–669.
[4] M. Carmo, D. L. Fritz, J. Mergel, D. Stolten, *Int. J. Hydrogen Energy* **2013**, *38*, 4901–4934.
[5] M. Wang, Z. Wang, X. Gong, Z. Guo, *Renewable Sustainable Energy Rev.* **2014**, *29*, 573–588.
[6] A. Marshall, B. Børresen, G. Hagen, M. Tsypkin, R. Tunold, *Energy* **2007**, *32*, 431–436.
[7] A. S. Aricò, S. Siracusano, N. Briguglio, V. Baglio, A. Di Blasi, V. Antonucci, *J. Appl. Electrochem.* **2013**, *43*, 107–118.
[8] A. Ursua, L. M. Gandía, P. Sanchis, *Proc. IEEE* **2012**, *100*, 410–426.
[9] P. Millet in *Compendium of Hydrogen Energy, Vol. 1* (Eds.: V. Subramani, A. Basile, T. N. Veziroğlu), Woodhead Publishing, Cambridge, **2015**, section 9.
[10] D. Tyagi, K. Scholz, S. Varma, K. Bhattacharya, S. Mali, P. S. Patil, S. R. Bharadwaj, *Int. J. Hydrogen Energy* **2012**, *37*, 3602–3611.
[11] B.-S. Lee, H.-Y. Park, I. Choi, M. K. Cho, H.-J. Kim, S. J. Yoo, D. Henkensmeier, J. Y. Kim, S. W. Nam, S. Park, K.-Y. Lee, J. H. Jang, *J. Power Sources* **2016**, *309*, 127–134.
[12] S. A. Grigoriev, P. Millet, V. N. Fateev, *J. Power Sources* **2008**, *177*, 281–285.
[13] G.-R. Xu, J.-J. Hui, T. Huang, Y. Chen, J.-M. Lee, *J. Power Sources* **2015**, *285*, 393–399.

© 2019 Wiley-VCH Verlag GmbH & Co. KGaA, Weinheim

[14] T. Yang, M. Du, H. Zhu, M. Zhang, M. Zou, *Electrochim. Acta* **2015**, *167*, 48 – 54.
[15] S. A. Grigoriev, M. S. Mamat, K. A. Dzhus, G. S. Walker, P. Millet, *Int. J. Hydrogen Energy* **2011**, *36*, 4143 – 4147.
[16] A. Stoyanova, G. Borisov, E. Lefterova, E. Slavcheva, *Int. J. Hydrogen Energy* **2012**, *37*, 16515 – 16521.
[17] Y. Matsumoto, E. Sato, *Mater. Chem. Phys.* **1986**, *14*, 397 – 426.
[18] E. Fabbri, A. Habereder, K. Waltar, R. Kötz, T. J. Schmidt, *Catal. Sci. Technol.* **2014**, *4*, 3800 – 3821.
[19] J. M. Hu, H. M. Meng, J. Q. Zhang, C. N. Cao, *Corr. Sci.* **2002**, *44*, 1655 – 1668.
[20] S. Trasatti, *J. Electroanal. Chem.* **1980**, *111*, 125 – 131.
[21] S. Trasatti, *Electrochim. Acta* **1984**, *29*, 1503 – 1512.
[22] C. C. McCrory, S. Jung, I. M. Ferrer, S. M. Chatman, J. C. Peters, T. F. Jaramillo, *J. Am. Chem. Soc.* **2015**, *137*, 4347 – 4357.
[23] M. Huynh, D. K. Bediako, D. G. Nocera, *J. Am. Chem. Soc.* **2014**, *136*, 6002 – 6010.
[24] N. Danilovic, R. Subbaraman, K. C. Chang, S. H. Chang, Y. J. Kang, J. Snyder, A. P. Paulikas, D. Strmcnik, Y. T. Kim, D. Myers, V. R. Stamenkovic, N. M. Markovic, *J. Phys. Chem. Lett.* **2014**, *5*, 2474 – 2478.
[25] E. A. Paoli, F. Masini, R. Frydendal, D. Deiana, C. Schlaup, M. Malizia, T. W. Hansen, S. Horch, I. E. Stephens, I. Chorkendorff, *Chem. Sci.* **2015**, *6*, 190 – 196.
[26] N. Hodnik, P. Jovanovic, A. Pavlisic, B. Jozinovic, M. Zorko, M. Bele, V. S. Šelh, M. Šala, S. Hocevar, M. Gaberscek, *J. Phys. Chem. C* **2015**, *119*, 10140 – 10147.
[27] S. Cherevko, S. Geiger, O. Kasian, N. Kulyk, J.-P. Grote, A. Savan, B. R. Shrestha, S. Merzlikin, B. Breitbach, A. Ludwig, K. J. J. Mayrhofer, *Catal. Today* **2016**, *262*, 170 – 180.
[28] E. J. M. O'Sullivan, J. R. White, *J. Electrochem. Soc.* **1989**, *136*, 2576 – 2583.
[29] A. Damjanovic, A. Dey, J. O. M. Bockris, *J. Electrochem. Soc.* **1966**, *113*, 739 – 746.
[30] Y. Lee, J. Suntivich, K. J. May, E. E. Perry, Y. Shao-Horn, *J. Phys. Chem. Lett.* **2012**, *3*, 399 – 404.
[31] P. C. K. Vesborg, T. F. Jaramillo, *RSC Adv.* **2012**, *2*, 7933 – 7947.
[32] J.-M. Hu, J.-Q. Zhang, C.-N. Cao, *Int. J. Hydrogen Energy* **2004**, *29*, 791 – 797.
[33] S. A. Grigoriev, A. A. Kalinnikov, *Int. J. Hydrogen Energy* **2017**, *42*, 1590 – 1597.
[34] S. A. Grigoriev, P. Millet, K. A. Dzhus, H. Middleton, T. O. Saetre, V. N. Fateev, *Int. J. Hydrogen Energy* **2010**, *35*, 5070 – 5076.
[35] C. Rozain, E. Mayousse, N. Guillet, P. Millet, *Appl. Catal. B* **2016**, *182*, 153 – 160.
[36] S. Cherevko, T. Reier, A. R. Zeradjanin, Z. Pawolek, P. Strasser, K. J. J. Mayrhofer, *Electrochem. Commun.* **2014**, *48*, 81 – 85.
[37] S. Fierro, A. Kapałka, C. Comninellis, *Electrochem. Commun.* **2010**, *12*, 172 – 174.
[38] A. Skulimowska, M. Dupont, M. Zaton, S. Sunde, L. Merlo, D. J. Jones, J. Rozière, *Int. J. Hydrogen Energy* **2014**, *39*, 6307 – 6316.
[39] G. Wei, Y. Wang, C. Huang, Q. Gao, Z. Wang, L. Xu, *Int. J. Hydrogen Energy* **2010**, *35*, 3951 – 3957.
[40] E. Rasten, G. Hagen, R. Tunold, *Electrochim. Acta* **2003**, *48*, 3945 – 3952.
[41] D. F. Abbott, D. Lebedev, K. Waltar, M. Povia, M. Nachtegaal, E. Fabbri, C. Coperet, T. J. Schmidt, *Chem. Mater.* **2016**, *28*, 6591 – 6604.
[42] S. D. Song, H. M. Zhang, X. P. Ma, Z. G. Shao, R. T. Baker, B. L. Yi, *Int. J. Hydrogen Energy* **2008**, *33*, 4955 – 4961.
[43] E. Mayousse, F. Maillard, F. F. Onana, O. Sicardy, N. Guillet, *Int. J. Hydrogen Energy* **2011**, *36*, 10474 – 10481.
[44] J. Xu, M. Wang, G. Liu, J. Li, X. Wang, *Electrochim. Acta* **2011**, *56*, 10223 – 10230.
[45] C. Felix, T. Maiyalagan, S. Pasupathi, B. Bladergroen, V. Linkov, *Micro Nanosyst.* **2012**, *4*, 186.
[46] J. C. Cruz, V. Baglio, S. Siracusano, R. Ornelas, L. Ortiz-Frade, L. G. Arriaga, V. Antonucci, A. S. Arico, *J. Nanopart. Res.* **2011**, *13*, 1639 – 1646.
[47] J. C. Cruz, V. Baglio, S. Siracusano, V. Antonucci, A. S. Aricò, R. Ornelas, L. Ortiz-Frade, G. Osorio-Monreal, S. M. Durón-Torres, L. G. Arriaga, *Int. J. Electrochem. Sci.* **2011**, *6*, 6607 – 6619.
[48] S. Siracusano, V. Baglio, A. Stassi, R. Ornelas, V. Antonucci, A. S. Arico, *Int. J. Hydrogen Energy* **2011**, *36*, 7822 – 7831.
[49] E. Slavcheva, I. Radev, S. Bliznakov, G. Topalov, P. Andreev, E. Budevski, *Electrochim. Acta* **2007**, *52*, 3889 – 3894.
[50] L. Ouattara, S. Fierro, O. Frey, M. Koudelka, C. Comninellis, *J. Appl. Electrochem.* **2009**, *39*, 1361 – 1367.
[51] P. Kúš, A. Ostroverkh, K. Ševčíková, I. Khalakhan, R. Fiala, T. Skála, N. Tsud, V. Matolin, *Int. J. Hydrogen Energy* **2016**, *41*, 15124 – 15132.
[52] P. Lettenmeier, J. Majchel, L. Wang, V. A. Saveleva, S. Zafeiratos, E. R. Savinova, J.-J. Gallet, F. Bournel, A. S. Gago, K. A. Friedrich, *Chem. Sci.* **2018**, *9*, 3570 – 3579.
[53] M. Sapountzi, S. C. Divane, E. I. Papaioannou, S. Souentie, C. G. Vayenas, *J. Electroanal. Chem.* **2011**, *662*, 116 – 122.
[54] B.-S. Lee, S. H. Ahn, H.-Y. Park, I. Choi, S. J. Yoo, H.-J. Kim, D. Henkensmeier, J. Y. Kim, S. Park, S. W. Nam, K.-Y. Lee, J. H. Jang, *Appl. Catal. B* **2015**, *179*, 285 – 291.
[55] G. Q. Li, S. T. Li, M. L. Xiao, J. J. Ge, C. P. Liu, W. Xing, *Nanoscale* **2017**, *9*, 9291 – 9298.
[56] E. Ortel, T. Reier, P. Strasser, R. Kraehnert, *Chem. Mater.* **2011**, *23*, 3201 – 3209.
[57] G. F. Li, H. M. Yu, W. Song, M. L. Dou, Y. K. Li, Z. G. Shao, B. L. Yi, *ChemSusChem* **2012**, *5*, 858.
[58] W. H. Lee, H. Kim, *Catal. Commun.* **2011**, *12*, 408 – 411.
[59] H.-S. Oh, H. N. Nong, T. Reier, M. Gliech, P. Strasser, *Chem. Sci.* **2015**, *6*, 3321 – 3328.
[60] Y. Pi, N. Zhang, S. Guo, J. Guo, X. Huang, *Nano Lett.* **2016**, *16*, 4424 – 4430.
[61] C. Zhao, H. Yu, Y. Li, X. Li, L. Ding, L. Fan, *J. Electroanal. Chem.* **2013**, *688*, 269 – 274.
[62] Y.-T. Kim, P. P. Lopes, S.-A. Park, A.-Y. Lee, J. Lim, H. Lee, S. Back, Y. Jung, N. Danilovic, V. Stamenkovic, J. Erlebacher, J. Snyder, N. M. Markovic, *Nat. Commun.* **2017**, *8*, 1449.
[63] P. P. Patel, M. K. Datta, O. I. Velikokhatnyi, R. Kuruba, K. Damodaran, P. Jampani, B. Gattu, P. M. Shanthi, S. S. Damle, P. N. Kumta, *Sci. Rep.* **2016**, *6*, 28367 – 28380.
[64] J. Roller, J. A. Jiménez, R. Jain, H. Yu, R. Maric, C. B. Carter, *J. Electrochem. Soc.* **2013**, *45*, 97.
[65] J. M. Roller, M. J. Arellano-Jimenez, R. Jain, H. Yu, C. B. Carter, R. Maric, *J. Electrochem. Soc.* **2013**, *160*, F716 – F730.
[66] T. Audichon, N. Mamaca, C. Morais, K. Servat, T. W. Napporn, E. Mayousse, N. Guillet, K. B. Kokoh, *ECS Trans.* **2013**, *45*, 47 – 58.
[67] N. Mamaca, E. Mayousse, S. Arrii-Clacens, T. W. Napporn, K. Servat, N. Guillet, K. B. Kokoh, *Appl. Catal. B* **2012**, *111*, 376 – 380.
[68] L. E. Owe, M. Tsypkin, K. S. Wallwork, R. G. Haverkamp, S. Sunde, *Electrochim. Acta* **2012**, *70*, 158 – 164.
[69] A. Di Blasi, C. D'Urso, V. Baglio, V. Antonucci, A. S. Arico, R. Ornelas, F. Matteucci, G. Orozco, D. Beltran, Y. Meas, L. G. Arriaga, *J. Appl. Electrochem.* **2009**, *39*, 191 – 196.
[70] J. B. Cheng, H. M. Zhang, G. B. Chen, Y. M. Zhang, *Electrochim. Acta* **2009**, *54*, 6250 – 6256.
[71] C. Felix, T. Maiyalagan, S. Pasupathi, B. Bladergroen, V. Linkov, *Int. J. Electrochem. Sci.* **2012**, *7*, 12064 – 12077.
[72] S. Siracusano, N. Van Dijk, E. Payne-Johnson, V. Baglio, A. S. Aricò, *Appl. Catal. B* **2015**, *164*, 488 – 495.
[73] R. Kötz, S. Stucki, *Electrochim. Acta* **1986**, *31*, 1311 – 1316.
[74] G. Lodi, E. Sivieri, A. Battisti, S. Trasatti, *J. Appl. Electrochem.* **1978**, *8*, 135 – 143.
[75] F. I. Mattos-Costa, P. de Lima-Neto, S. A. S. Machadoa, L. A. Avaca, *Electrochim. Acta* **1998**, *44*, 1515 – 1523.
[76] C. Angelinetta, S. Trasatti, L. D. Atanasoska, Z. S. Minevski, R. T. Atanasoski, *Mater. Chem. Phys.* **1989**, *22*, 231 – 247.
[77] S. Siracusano, V. Baglio, E. Moukheiber, L. Merlo, A. S. Arico, *Int. J. Hydrogen Energy* **2015**, *40*, 14430 – 14435.
[78] F. Hegge, R. Moroni, P. Trinke, B. Bensmann, R. H. Rauschenbach, S. Thiele, S. Vierrath, *J. Power Sources* **2018**, *393*, 62 – 66.
[79] S. Siracusano, V. Baglio, N. Van Dijk, L. Merlo, A. S. Aricò, *Appl. Energy* **2017**, *192*, 477 – 489.
[80] Y. Murakami, S. Tsuchiya, K. Yahikozawa, Y. Takasu, *J. Mater. Sci. Lett.* **1994**, *13*, 1773 – 1774.
[81] M. Ito, Y. Murakami, H. Kaji, H. Ohkawauch, K. Yahikozawa, Y. Takasu, *J. Electrochem. Soc.* **1994**, *141*, 1243 – 1245.
[82] N. Danilovic, R. Subbaraman, K. C. Chang, S. H. Chang, Y. Kang, J. Snyder, A. P. Paulikas, D. Strmcnik, Y. T. Kim, D. Myers, V. R. Stamen-

© 2019 Wiley-VCH Verlag GmbH & Co. KGaA, Weinheim

kovic, N. M. Markovic, *Angew. Chem. Int. Ed.* **2014**, *53*, 14016 – 14021; *Angew. Chem.* **2014**, *126*, 14240 – 14245.
[83] T. Audichon, E. Mayousse, S. Morisset, C. Morais, C. Comminges, T. W. Napporn, K. B. Kokoh, *Int. J. Hydrogen Energy* **2014**, *39*, 16785 – 16796.
[84] O. Kasian, S. Geiger, P. Stock, G. Polymeros, B. Breitbach, A. Savan, A. Ludwig, S. Cherevko, K. J. J. Mayrhofer, *J. Electrochem. Soc.* **2016**, *163*, F3099 – F3104.
[85] V. A. Saveleva, L. Wang, W. Luo, S. Zafeiratos, C. U. Bouillet, A. S. Gago, K. A. Friedrich, E. R. Savinova, *J. Phys. Chem. Lett.* **2016**, *7*, 3240 – 3245.
[86] Z. Ma, Y. Zhang, S. Liu, W. Xu, L. Wu, Y. Hsieh, P. Liu, Y. Zhu, K. Sasaki, J. N. Renner, K. E. Ayers, R. R. Adzic, J. X. Wang, *J. Electroanal. Chem.* **2018**, *819*, 296 – 305.
[87] G. Li, S. Li, J. Ge, C. Liu, W. Xing, *J. Mater. Chem. A* **2017**, *5*, 17221 – 17229.
[88] T. Audichon, T. W. Napporn, C. Canaff, C. Morais, C. Comminges, K. B. Kokoh, *J. Phys. Chem. C* **2016**, *120*, 2562 – 2573.
[89] E. Antolini, *ACS Catal.* **2014**, *4*, 1426 – 1440.
[90] R. Hutchings, K. Müller, R. Kötz, S. Stucki, *J. Mater. Sci.* **1984**, *19*, 3987 – 3994.
[91] A. T. Marshall, S. Sunde, M. Tsypkin, R. Tunold, *Int. J. Hydrogen Energy* **2007**, *32*, 2320 – 2324.
[92] A. Marshall, B. Børresen, G. Hagen, M. Tsypkin, R. Tunold, *Mater. Chem. Phys.* **2005**, *94*, 226 – 232.
[93] A. Marshall, B. Børresen, G. Hagen, M. Tsypkin, R. Tunold, *Electrochim. Acta* **2006**, *51*, 3161 – 3167.
[94] S. Lin, T. Wen, *J. Electrochem. Soc.* **1993**, *140*, 2265 – 2271.
[95] K. Kameyama, K. Tsukada, K. Yahikozawa, K. Y. Takasu, *J. Electrochem. Soc.* **1994**, *141*, 643 – 647.
[96] J. Cheng, H. Zhang, H. Ma, H. Zhong, Y. Zou, *Int. J. Hydrogen Energy* **2009**, *34*, 6609 – 6613.
[97] J. Corona-Guinto, L. Cardeno-Garcia, D. C. Martinez-Casillas, J. M. Sandoval-Pineda, P. Tamayo-Meza, R. Silva-Casarin, R. G. Gonzalez-Huerta, *Int. J. Hydrogen Energy* **2013**, *38*, 12667 – 12673.
[98] T. Audichon, S. Morisset, T. W. Napporn, K. B. Kokoh, C. Comminges, C. Morais, *ChemElectroChem* **2015**, *2*, 1128 – 1137.
[99] S.-Y. Lee, B.-J. Kim, S.-J. Park, *Energy* **2014**, *66*, 70 – 76.
[100] C. Xu, L. Ma, J. Li, W. Zhao, Z. Gan, *Int. J. Hydrogen Energy* **2012**, *37*, 2985 – 2992.
[101] S. Ardizzone, C. L. Bianchi, L. Borgese, G. Cappelletti, C. Locatelli, A. Minguzzi, S. Rondinini, A. Vertova, P. C. Ricci, C. Cannas, A. Musinu, *J. Appl. Electrochem.* **2009**, *39*, 2093 – 2105.
[102] G. Li, H. Yu, X. Wang, S. Sun, Y. Li, Z. Shao, B. Yi, *Phys. Chem. Chem. Phys.* **2013**, *15*, 2858 – 2866.
[103] J. Xu, G. Liu, J. Li, X. Wang, *Electrochim. Acta* **2012**, *59*, 105 – 112.
[104] Y. Murakami, H. Ohkawauchi, M. Ito, K. Yahikozawa, Y. Takasu, *Electrochim. Acta* **1994**, *39*, 2551 – 2554.
[105] C. P. De Pauli, S. Trasatti, *J. Electroanal. Chem.* **2002**, *538*, 145 – 151.
[106] A. Marshall, M. Tsypkin, B. Børresen, G. Hagen, R. Tunold, *J. New Mater. Electrochem. Syst.* **2004**, *7*, 197 – 204.
[107] A. Marshall, B. Børresen, G. Hagen, S. Sunde, M. Tsypkin, *Russ. J. Electrochem.* **2006**, *42*, 1134 – 1140.
[108] J. Y. Lim, G. Rahman, S. Y. Chae, K. Lee, C. Kim, O. Joo, *Int. J. Energy Res.* **2014**, *38*, 875 – 883.
[109] X. Wu, J. Tayal, S. Basu, K. Scott, *Int. J. Hydrogen Energy* **2011**, *36*, 14796 – 14804.
[110] N. J. Pérez-Viramontes, I. L. Escalante-Garcia, C. Guzmán-Martinez, M. Galvan-Valencia, S. M. Duron-Torres, *J. Appl. Electrochem.* **2015**, *45*, 1165 – 1173.
[111] S. Ardizzone, C. L. Bianchi, G. Cappelletti, M. Ionita, A. Minguzzi, S. Rondinini, A. Vertova, *J. Electroanal. Chem.* **2006**, *589*, 160 – 166.
[112] K. Kadakia, M. K. Datta, O. I. Velikokhatnyi, P. Jampani, S. K. Park, P. Saha, J. A. Poston, A. Manivannan, P. N. Kumta, *Int. J. Hydrogen Energy* **2012**, *37*, 3001 – 3013.
[113] O. Kasian, S. Geiger, M. Schalenbach, A. M. Mingers, A. Savan, A. Ludwig, S. Cherevko, K. J. J. Mayrhofer, *Electrocatalysis* **2018**, *9*, 139 – 145.
[114] J. Xu, Q. Li, E. Christensen, X. Wang, N. J. Bjerrum, *Int. J. Electrochem. Sci.* **2013**, *8*, 2388 – 2406.
[115] O. I. Velikokhatnyi, K. Kadakia, M. K. Datta, P. N. Kumta, *J. Phys. Chem. C* **2013**, *117*, 20542 – 20547.
[116] K. Kadakia, M. K. Datta, P. H. Jampani, S. K. Park, P. N. Kumta, *J. Power Sources* **2013**, *222*, 313 – 317.
[117] K. S. Kadakia, P. H. Jampani, O. I. Velikokhatnyi, M. K. Datta, S. K. Park, D. H. Hong, S. J. Chung, P. N. Kumta, *J. Power Sources* **2014**, *269*, 855 – 865.
[118] M. K. Datta, K. Kadakia, O. I. Velikokhatnyi, P. H. Jampani, S. J. Chung, J. A. Poston, A. Manivannan, P. N. Kumta, *J. Mater. Chem. A* **2013**, *1*, 4026 – 4037.
[119] K. S. Kadakia, P. Jampani, O. I. Velikokhatnyi, M. K. Datta, S. J. Chung, J. A. Poston, A. Manivannan, P. N. Kumta, *J. Electrochem. Soc.* **2014**, *161*, F868 – F875.
[120] K. Kadakia, M. K. Datta, O. I. Velikokhatnyi, P. H. Jampani, P. N. Kumta, *Int. J. Hydrogen Energy* **2014**, *39*, 664 – 674.
[121] K. Kadakia, M. K. Datta, O. I. Velikokhatnyi, P. Jampani, S. K. Park, S. J. Chung, P. N. Kumta, *J. Power Sources* **2014**, *245*, 362 – 370.
[122] S. D. Yim, W. Y. Lee, Y. G. Yoon, Y. J. Sohn, G. G. Park, T. H. Yang, C. S. Kim, *Electrochim. Acta* **2004**, *50*, 713 – 718.
[123] F. Ye, J. Li, X. Wang, T. Wang, S. Li, H. Wei, Q. Li, E. Christensen, *Int. J. Hydrogen Energy* **2010**, *35*, 8049 – 8055.
[124] L. A. Da Silva, V. A. Alves, S. Trasatti, J. F. C. Boodts, *J. Electroanal. Chem.* **1997**, *427*, 97 – 104.
[125] D. Seley, K. Ayers, B. A. Parkinson, *ACS Comb. Sci.* **2013**, *15*, 82 – 89.
[126] M. H. P. Santana, L. D. Faria, J. F. Boodts, *J. Appl. Electrochem.* **2005**, *35*, 915 – 924.
[127] A. Bonakdarpour, R. T. Tucker, M. D. Fleischauer, N. A. Beckers, M. J. Brett, D. P. Wilkinson, *Electrochim. Acta* **2012**, *85*, 492 – 500.
[128] L. Zhang, L. Y. Wang, C. M. B. Holt, T. Navessin, K. Malek, M. H. Eikerling, D. Mitlin, *J. Phys. Chem. C* **2010**, *114*, 16463 – 16474.
[129] M. Yin, J. Xu, Q. Li, J. O. Jensen, Y. Huang, L. N. Cleemann, N. J. Bjerrum, W. Xing, *Appl. Catal. B* **2014**, *144*, 112 – 120.
[130] X. Wu, K. Scott, *Int. J. Hydrogen Energy* **2011**, *36*, 5806 – 5810.
[131] A. T. Marshall, R. G. Haverkamp, *Electrochim. Acta* **2010**, *55*, 1978 – 1984.
[132] J. C. Cruz, S. Rivas, D. Beltran, Y. Meas, R. Ornelas, G. Osorio-Monreal, L. Ortiz-Frade, J. Ledesma-Garcia, L. G. Arriaga, *Int. J. Hydrogen Energy* **2012**, *37*, 13522 – 13528.
[133] V. K. Puthiyapura, M. Mamlouk, S. Pasupathi, B. G. Pollet, K. Scott, *J. Power Sources* **2014**, *269*, 451 – 460.
[134] H. S. Oh, H. N. Nong, P. Strasser, *Adv. Funct. Mater.* **2015**, *25*, 1074 – 1081.
[135] H. N. Nong, L. Gan, E. Willinger, D. Teschner, P. Strasser, *Chem. Sci.* **2014**, *5*, 2955 – 2963.
[136] H. N. Nong, H.-S. Oh, T. Reier, E. Willinger, M.-G. Willinger, V. Petkov, D. Teschner, P. Strasser, *Angew. Chem.* **2015**, *127*, 3018 – 3022.
[137] H.-S. Oh, H. N. Nong, T. Reier, A. Bergmann, M. Gliech, J. F. de Araújo, E. Willinger, R. Schlögl, D. Teschner, P. Strasser, *J. Am. Chem. Soc.* **2016**, *138*, 12552 – 12563.
[138] J. Tong, Y. Liu, Q. Peng, W. Hu, Q. Wu, *J. Mater. Sci.* **2017**, *52*, 13427 – 13443.
[139] F. Karimi, B. A. Peppley, *Electrochim. Acta* **2017**, *246*, 654 – 670.
[140] F. Karimi, A. Bazylak, B. A. Peppley, *J. Electrochem. Soc.* **2017**, *164*, F464 – F474.
[141] L. Wang, F. Song, G. Ozouf, D. Geiger, T. Morawietz, M. Handl, P. Gazdzicki, C. Beauger, U. Kaiser, R. Hiesgen, A. S. Gago, K. A. Friedrich, *J. Mater. Chem. A* **2017**, *5*, 3172 – 3178.
[142] K.-S. Lee, I.-S. Park, Y.-H. Cho, D.-S. Jung, N. Jung, H.-Y. Park, Y.-E. Sung, *J. Catal.* **2008**, *258*, 143 – 152.
[143] S. Gurrik, M.Sc. thesis, Norwegian University of Science and Technology, **2012**.
[144] A. T. Marshall, R. G. Haverkamp, *J. Mater. Sci.* **2012**, *47*, 1135 – 1141.
[145] P. Mazúr, J. Polonský, M. Paidar, K. Bouzek, *Int. J. Hydrogen Energy* **2012**, *37*, 12081 – 12088.
[146] E. Oakton, D. Lebedev, M. Povia, D. F. Abbott, E. Fabbri, A. Fedorov, M. Nachtegaal, C. Coperet, T. J. Schmidt, *ACS Catal.* **2017**, *7*, 2346 – 2352.
[147] Z.-X. Lu, Y. Shi, C.-F. Yan, C.-Q. Guo, Z.-D. Wang, *Int. J. Hydrogen Energy* **2017**, *42*, 3572 – 3578.
[148] E. Oakton, D. Lebedev, A. Fedorov, F. Krumeich, J. Tillier, O. Sereda, T. J. Schmidt, C. P. Coperet, *New J. Chem.* **2016**, *40*, 1834 – 1838.
[149] S. L. Gojkovic, B. M. Babic, V. R. Radmilovic, N. V. Krstajic, *J. Electroanal. Chem.* **2010**, *639*, 161 – 166.
[150] G. Wu, M. A. Nelson, N. H. Mack, S. G. Ma, P. Sekhar, F. H. Garzon, P. Zelenay, *Chem. Commun.* **2010**, *46*, 7489 – 7491.

© 2019 Wiley-VCH Verlag GmbH & Co. KGaA, Weinheim

[151] S. von Kraemer, J. Wikander, G. Lindbergh, A. Lundblad, A. E. C. Palmqvist, *J. Power Sources* **2008**, *180*, 185 – 190.
[152] J. R. Osman, J. A. Crayston, A. Pratt, D. T. Richens, *J. Sol – Gel Sci. Technol.* **2008**, *46*, 126 – 132.
[153] J. R. Osman, J. A. Crayston, A. Pratt, D. T. Richens, *J. Sol – Gel Sci. Technol.* **2007**, *44*, 219 – 225.
[154] C. Rozain, E. Mayousse, N. Guillet, P. Millet, *Appl. Catal. B* **2016**, *182*, 123 – 160.
[155] C. H. Comninellis, G. P. Vercesi, *J. Appl. Electrochem.* **1991**, *21*, 335 – 345.
[156] K. Kameyama, S. Shohji, S. Onoue, K. Nishimura, K. Yahikozawa, Y. Takasu, *J. Electrochem. Soc.* **1993**, *140*, 1034 – 1037.
[157] B. Johnson, F. Girgsdies, G. Weinberg, D. Rosenthal, A. Knop-Gericke, R. Schlögl, T. Reier, P. Strasser, *J. Phys. Chem. C* **2013**, *117*, 25443 – 25450.
[158] Z. Chen, S. Zhang, Y. Shao, S. Zhou, X. Wu, J. Zhu, D. Tang, *Appl. Surf. Sci.* **2017**, *422*, 891 – 899.
[159] S. Siracusano, V. Baglio, C. D'Urso, V. Antonucci, A. S. Aricò, *Electrochim. Acta* **2009**, *54*, 6292 – 6299.
[160] E. Slavcheva, G. Borisov, E. Lefterova, E. Petkucheva, I. Boshnakova, *Int. J. Hydrogen Energy* **2015**, *40*, 11356 – 11361.
[161] L. Wang, P. Lettenmeier, U. G. Schindler, P. Gazdzicki, N. A. Canas, T. Morawietz, R. Hiesgen, S. S. Hosseiny, A. S. Gago, K. A. Friedrich, *Phys. Chem. Chem. Phys.* **2016**, *18*, 4487 – 4495.
[162] C. Hao, H. Lv, C. Mi, Y. Song, J. Ma, *ACS Sustainable Chem. Eng.* **2016**, *4*, 746 – 756.
[163] W. Hu, S. Chen, Q. Xia, *Int. J. Hydrogen Energy* **2014**, *39*, 6967 – 6976.
[164] J. Pettersson, B. Ramsey, D. Harrison, *J. Power Sources* **2006**, *157*, 28 – 34.
[165] C. Hao, H. Lv, Q. Zhao, *Int. J. Hydrogen Energy* **2017**, *42*, 9384 – 9395.
[166] V. K. Puthiyapura, S. Pasupathi, H. Su, X. Liu, B. Pollet, K. Scott, *Int. J. Hydrogen Energy* **2014**, *39*, 1905 – 1913.
[167] M. Yagi, E. Tomita, S. Sakita, T. Kuwabara, K. Nagai, *J. Phys. Chem. B* **2005**, *109*, 21489 – 21491.
[168] S. Sui, L. Ma, Y. Zhai, *J. Chem. Eng.* **2009**, *4*, 8 – 11.
[169] L. Ma, S. Sui, Y. Zhai, *Int. J. Hydrogen Energy* **2009**, *34*, 678 – 684.
[170] J. Polonský, P. Mazúr, M. Paidar, E. Christensen, K. Bouzek, *Int. J. Hydrogen Energy* **2014**, *39*, 3072 – 3078.
[171] Z. Yan, H. Zhang, Z. Feng, M. Tang, X. Yuan, Z. Tan, *J. Alloys Compd.* **2017**, *708*, 1081 – 1088.
[172] J. Polonský, I. M. Petrushina, E. Christensen, K. Bouzek, C. B. Prag, J. E. T. Andersen, N. J. Bjerrum, *Int. J. Hydrogen Energy* **2012**, *37*, 2173 – 2181.
[173] A. V. Nikiforov, A. L. T. Garcia, I. M. Petrushina, E. Christensen, N. J. Bjerrum, *Int. J. Hydrogen Energy* **2011**, *36*, 5797 – 5805.
[174] N. Baumann, C. Cremers, K. Pinkwart, J. Tübke, *Energy Technol.* **2016**, *4*, 212 – 220.
[175] D. L. Wang, C. V. Subban, H. S. Wang, E. Rus, F. J. DiSalvo, H. D. Abruna, *J. Am. Chem. Soc.* **2010**, *132*, 10218 – 10220.
[176] H. Chhina, S. Campbell, O. Kesler, *J. Electrochem. Soc.* **2007**, *154*, B533 – B539.
[177] F. Kong, S. Zhang, G.-P. Yin, J. Liu, Z. Q. Xu, *Int. J. Hydrogen Energy* **2013**, *38*, 9217 – 9222.
[178] L. Wang, V. A. Saveleva, S. Zafeiratos, E. R. Savinova, P. Lettenmeier, P. Gazdzicki, A. S. Gago, K. A. Friedrich, *Nano Energy* **2017**, *34*, 385 – 391.
[179] L. C. Seitz, C. F. Dickens, K. Nishio, Y. Hikita, J. Montoya, A. Doyle, C. Kirk, A. Vojvodic, H. Y. Hwang, J. K. Norskov, T. F. Jaramillo, *Science* **2016**, *353*, 1011 – 1014.
[180] O. Diaz-Morales, S. Raaijman, R. Kortlever, P. J. Kooyman, T. Wezendonk, J. Gascon, W. T. Fu, M. T. M. Koper, *Nat. Commun.* **2016**, *7*, 12363.
[181] T. Reier, Z. Pawolek, S. Cherevko, M. Bruns, T. Jones, D. Teschner, S. Selve, A. Bergmann, H. N. Nong, R. Schlögl, K. J. J. Mayrhofer, P. Strasser, *J. Am. Chem. Soc.* **2015**, *137*, 13031 – 13040.
[182] V. Pfeifer, T. E. Jones, J. J. V. Vélez, R. Arrigo, S. Piccinin, M. Hävecker, A. K. Gericke, R. Schlögl, *Chem. Sci.* **2017**, *8*, 2143 – 2149.
[183] A. Grimaud, A. Demortière, M. Saubanère, W. Dachraoui, M. Duchamp, M.-L. Doublet, J.-M. Tarascon, *Nat. Energy* **2016**, *2*, 16189.
[184] S. Geiger, O. Kasian, M. Ledendecker, E. Pizzutilo, A. M. Mingers, W. T. Fu, O. D. Morales, Z. Li, T. Oellers, L. Fruchter, A. Ludwig, K. J. J. Mayrhofer, M. T. M. Koper, S. Cherevko, *Nat. Catal.* **2018**, *1*, 508 – 515.
[185] G. Beni, L. M. Schiavone, J. L. Shay, W. C. Dautremont-Smith, B. S. Schneider, *Nature* **1979**, *282*, 281 – 283.
[186] E. J. Frazer, R. Woods, *J. Electroanal. Chem. Interfacial Electrochem.* **1979**, *102*, 127 – 130.
[187] M. Vukovic, *J. Appl. Electrochem.* **1987**, *17*, 737 – 745.
[188] T. Reier, D. Teschner, T. Lunkenbein, A. Bergmann, S. Selve, R. Kraehnert, R. Schlögl, P. Strasser, *J. Electrochem. Soc.* **2014**, *161*, F876 – F882.
[189] V. Pfeifer, T. E. Jones, J. J. V. Velez, C. Massu8, R. Arrigo, D. Teschner, F. Girgsdies, M. Scherzer, M. T. Greiner, J. Allan, M. Hashagen, G. Weinberg, S. Piccinin, M. Haevecker, A. Knop-Gericke, R. Schlögl, *Surf. Interface Anal.* **2016**, *48*, 261 – 273.
[190] V. Pfeifer, T. E. Jones, J. J. V. Velez, C. Massu, M. T. Greiner, R. Arrigo, D. Teschner, F. Girgsdies, M. Scherzer, J. Allan, M. Hashagen, G. Weinberg, S. Piccinin, M. Haevecker, A. Knop-Gericke, R. Schlögl, *Phys. Chem. Chem. Phys.* **2016**, *18*, 2292 – 2296.
[191] V. Pfeifer, T. E. Jones, S. Wrabetz, C. Massue, J. J. V. Velez, R. Arrigo, M. Scherzer, S. Piccinin, M. Havecker, A. Knop-Gericke, R. Schlögl, *Chem. Sci.* **2016**, *7*, 6791 – 6795.
[192] S. Geiger, O. Kasian, B. R. Shrestha, A. M. Mingers, K. J. J. Mayrhofer, S. Cherevko, *J. Electrochem. Soc.* **2016**, *163*, F3132 – F3138.
[193] E. Willinger, C. Massué, R. Schlögl, M. G. Willinger, *J. Am. Chem. Soc.* **2017**, *139*, 12093 – 12101.
[194] C. Massué, X. Huang, A. Tarasov, C. Ranjan, S. Cap, R. Schlögl, *ChemSusChem* **2017**, *10*, 1958 – 1968.
[195] Z. Pavlovic, C. Ranjan, M. Van Gastel, R. Schlögl. *Chem. Commun.* **2017**, *53*, 12414 – 12417.

Manuscript received: December 9, 2018
Revised manuscript received: January 15, 2019
Accepted manuscript online: January 17, 2019
Version of record online: April 1, 2019

© 2019 Wiley-VCH Verlag GmbH & Co. KGaA, Weinheim